Review—High-Pressure Carbon Dioxide Separation Using Ionic Liquids: A CO_2-Electrocatalysis Perspective

To cite this article: Andressa Mota-Lima *et al* 2021 *J. Electrochem. Soc.* **168** 086502

View the article online for updates and enhancements.

Review—High-Pressure Carbon Dioxide Separation Using Ionic Liquids: A CO₂-Electrocatalysis Perspective

Andressa Mota-Lima,[1,z] Murilo Leite Alcantara,[1] Fernando J. Pérez-Sanz,[2] Reinaldo C. Bazito,[2] Pedro Vidinha,[2] Rita M. B. Alves,[1] and Claudio A. Oller Nascimento[1]

[1]Department of Chemical Engineering; Escola Politécnica, Universidade de São Paulo, Av. Prof. Luciano Gualberto 380, São Paulo, SP 05508-010, Brazil
[2]Institute of Chemistry, Universidade de São Paulo, Av. Prof. Lineu Prestes 748, São Paulo, SP 5508-000, Brazil

The use of methane as the energy vector in our current energy matrix has challenged scientists to solve problems, which are now related to the exploration of oil wells but tomorrow will be the foundation for a carbon-neutral industry. Subsea exploration challenges engineers to find new solutions to separate CO_2 from CH_4 at the extremely high pressure of ca. 400 bar, to which all mature separation technologies are unsuitable. In this review, we highlight possible ways to employ ionic liquid (IL) as a highly selective absorbent to CO_2 for extremely high pressure. Besides revising the high-pressure physical-chemical properties of ILs, the IL designing principles, and finally, the current employment of IL for preparing membranes, we prospect possible solutions for the sluggish, disfavored IL-regeneration at high pressure. We prospect—CO_2 electro-reduction reaction (CO_2RR) as a promising disruption for separation processes, being CO_2RR-based technologies viable not only for IL-regeneration after the IL-based CO_2 capture but also for CO_2 conversion into valuable fuels/chemicals. As a prelude to CO_2RR-based technologies, this review highlights key aspects concerning the use of IL as the electrolyte in an electrochemical cell performing CO_2RR.

List of Symbols

AEP	1-(2-aminoethyl) piperazine
[amim][DCA]	1-Allyl-3-methylimidazolium dicyanamide
[Apbim][BF4]	1-(3-propilamino)−3-butylimidazolium tetrafluoroborate
[BA][For]	butylammonium formate
[BA][Ac]	n-butylammonium acetate
[BA][N]	n-butylammonium nitrate
[BHEA][For]	N-butyl-2-hydroxyethylammonium formate
[BHEA] [Ac]	N-butyl-2-hydroxyethylammonium acetate
[BHEA][Pro]	N-butyl-2-hydroxyethylammonium propionate
[BHEA][But]	N-butyl-2-hydroxyethylammonium butanoate
[BHEA][Pent]	N-butyl-2-hydroxyethylammonium pentanoate
[bmim]	
[bmpip][Tf2N]	1-Butyl-1-methylpiperidinium bis(trifluoromethylsulfonyl)imide
[bmpyrr][DCA]	1-Butyl-1-methylpyrrolidinium dicyanamide
[cprop][DCA]	1,2,3-Tris-(diethylamino)cyclopropenylium dicyanamide
[cprop][Tf2N]	1,2,3-Tris(diethylamino)cyclopropenylium bis(trifluoromethylsulfonyl)imide
[C2mim][Ac]	1-ethyl-3-methylimidazolium acetate
[C2mim][BF4]	1-bu-tylpyridinium, and bis(trifluoromethylsulfonyl)imide
[C2mim][CH₃OHPO₂]	1-ethyl-3-methylimidazolium methylphosphonate
[C2mim][CH₃SO₃]	1-ethyl-3-methylimidazolium methanesulfonate
[C₂mim][CF₃SO₃]	1-ethyl-3-methylimidazolium trifluoromethanesulfonate (triflate)
[C2mim][N(CN)₂]	1-ethyl-3-methylimidazolium dicyanamide
[C2mim][(OCH₃)₂PO₂]	1-ethyl-3-methylimidazolium dimethylphosphate
[C2mim][OTf]	1-etyl-3-methyl-imidazolium trifluoromethanesulfonate
[C2mim][SCN]	1-ethyl-3-methylimidazolium thiocyanate
[C2mim][TFSI]	1-butylpyridinium tetrafluoroborate
[C2mim][Tos]	1-ethyl-3-methylimidazolium tosylate
[C2mim][FSA]	1-ethyl-3-methylimidazolium (fluorosulfonyl)amide
[C2Pip][HSO4]	1-methylpiperidinium sulfate
[C2Pyr][CF3COO]	1-methylpyrrolidinium trifluoroacetate
[C2Pyr][F]	1-methylpyrrolidinium formate
[C2Pyr][HSO4]	1-methylpyrrolidinium sulfate
[C4mim] [Ac]	1-butyl-3-methyl-imidazolium acetate
[C4mim][PF6]	1-n-butyl-3-methylimidazolium hexafluoro-phosphat
[C4mim][MeSO4]	1-butyl-3-methylimidazolium methylsulfate;
[C4mim][SCN]	1-butyl-3-methylimidazolium thiocyanate
[C4mPy][SCN]	1-butyl-4-methylpyridinium thiocyanate
[C4mPyr][SCN]	1-butyl-1-methylpyrrolidinium thiocyanate
[C4mPip][SCN]	1-butyl-1-methylpiperidinium thiocyanate
[C4mim][TFA]	1-butyl-3-methylimidazolium trifluoroacetate
[C4mim][TFSI]	1-butyl-3-methyl-imidazolium bis(trifluoromethylsulfonyl)imide
[C4Py][TFSI]	1-ethyl-3-methylimidazolium tetrafluoroborate
[C4Py][BF4]	1-ethyl-3-methylimidazolium bis(trifluoromethylsulfonyl)imide
[C6mim][Tf2N]	1-hexyl-3-methylimidazolium bis(trifluoromethylsulfonyl)imide
ChCl	2-Hydroxyethyl-trimethylammonium chloride (Choline chloride)
[DBU] [TFSI]	1,8-diazabicyclo[5,4,0]−7-ene bis(trifluoromethylsulfonyl)imide

ᶻE-mail: mota@usp.br; abmlima@gmail.com

[DEA][Ac]	diethylammonium acetate
[DEA][Bu]	diethylammonium butanoate
[DEA][Cl]	diethylammonium chloride
[DEA][For]	diethylammonium formate
DEA	Diethanolamine
[DPA][For]	di-n-propylammonium formate
[DEA][HSO$_4$]	diethylammonium sulfate
[DEA][OSA]	diethylammonium sulfamate
[D2HEA][Pe]	2-hydroxy diethylammonium pentanoate
[EA][Bu]	ethylammonium butyrate
[EA][Gly]	ethylammonium glycolate
[EA][Lac]	ethylammonium lactate
[EA][HS]	ethylammonium hydrogen sulfate
[EA][For]	ethylammonium formate
[EA][N]	ethanolammonium nitrate
[EA][P]	ethylammonium propionate
[emim][DEP]	1-Ethyl-3-methylimidazolium diethylphosphate
[emim]	
EG	Ethylene glycol
[EOA][N]	ethanolammonium nitrate
[EOA][For]	ethanolammonium formate
[EOA][Lac]	ethanolammonium lactate
[EOA][Ac]	ethanolammonium acetate
[HEA][Pe]	2-hydroxy triethylammonium pentanoate
[2HEA][But]	2-hydroxyethylammonium butanoate
[2HEA][Pe]	2-hydroxy ethylammonium pentanoate
[HDBU][Im]	1,8-Diazabicyclo[5.4.0]undec-7-ene
[MA][For]	3-methylbutylammonium formate
MEA	Monoethanolamine
MDEA	methyldiethanolamine
[2MPA][For]	2-methylpropylammonium formate
[2MBA][For]	2-methylbutylammonium formate
[MMpy][eFAP]	1,3-dimethylpyridinium tris(pentafluoroethyl)
[m-2HEA][Pr]	N-methyl-2-hydroxyethylammonium
[N4111][NTf2]	butyl-trimethyl-ammonium bis(trifluoromethylsulfonyl)imide
[Pip][F]	Piperidinium formate
Reline	
scCO$_2$	CO$_2$ at the supercritical conditions
[tes][Tf2N]	Triethylsulfonium bis(trifluoromethylsulfonyl)imid
[tEtA][For]	triethylammonium formate
[tEtA][Ac]	triethylammonium acetate
[TFSI]	
[thtdp][DCA]	Trihexyltetradecylphosphonium dicyanamide
[thtdp][PF$_6$]	trihexyl(tetradecyl)phosphonium hexafluoro-phosphate
[P$_{4442}$][IDA]	Tri-n-butyl(ethyl)phosphonium iminodiacetate
[PeA][For]	pentylammonium formate
[2POA][For]	2-propanolammonium formate

The petroleum industry has explored subsea natural gas reservoirs, and the fluid found in Brazil has a substantially high CO$_2$ content,[1] being CO$_2$ currently separated and buried into the reservoir. However, transporting crude gas from the seafloor to the ocean surface substantially adds to the cost of recovering natural gas (mostly composed of CH$_4$), especially in deep waters, whose depths reach at least 2 Km. Figure 1 drafts the conceptual idea of a subsea separation unit. To date, such unit separates the streaming coming from the reservoir wells into three final phases, namely water, oil, and gas, being the water discharged into the injection wells, whereas both oil and crude gas transported up to the floating unit on the surface, where the CH$_4$/CO$_2$ mixture is currently separated. If CO$_2$ could be removed from crude gas by an extra unit still on the seafloor, instead of on the sea surface, the cost of piping to transport

either the crude gas up or the CO$_2$ down could be reduced. The extremely high pressure on the seafloor, however, imposes peculiar constrictions over the separation processes.[2] In this review, we survey possible ways of using ionic liquids (ILs) for this separation, highlighting the key fundamental aspects for that aim, such as high-pressure solubilities, phase diagrams, etc. Moreover, we foresee CO$_2$ electrocatalysis as a possible tool not only for assisting CO$_2$ separation with ILs but also to pave new ways in the context of the carbon-neutral industry.

Seafloor separation technologies must be compact, of low maintenance, and, above all, reliable at 400 bar or other higher external pressures found on the seafloor. Traditional CO$_2$ removal technologies,[4,5] such as aqueous amine scrubbing, are unsuitable for such applications. Additionally, the most mature membrane-based technologies are not suitable for the subsea application, either, because parts of the device, such as the vacuum pump are not applicable to the subsea operation. These technologies have to be imperatively innovated to serve the purpose of CO$_2$ separation at pressures varying from 200 to 400 bars and at temperatures ranging from 20 °C to 100 °C, which are variations allowed in seafloor conditions. Ionic Liquids (IL) employment for CO$_2$-CH$_4$ separation has gained attention just recently, given widely-known IL suitability for extraction up to 400 bar.[6] The negligible vapor pressure, the high thermal stability, and tunable molecular structures make IL a promising candidate to replace the conventional aqueous ethanolamine solvents. In principle, not only CO$_2$ but also other undesirable oil/gas contaminants, such as H$_2$S, can be removed from high-pressure streaming with ionic liquids.[7] There are more opportunities than simply CO$_2$ separation with IL on the seafloor, and any real technical advance in this respect may trigger a number of others.

At high pressure, ILs have been reported to have high CO$_2$ absorption[8] and high CO$_2$ selectivity over CH$_4$.[9–11] However, most of these data were obtained with modeling predictions, and physical proof of concept for CO$_2$/CH$_4$ separation at high pressure remains to be produced. There are plenty of IL reviews on varied topics, such as the solubility in ILs,[12] multiscale modelings on ILs,[13] the CO$_2$ capture by ILs,[14] structure-property relationships,[15] and the separation of light hydrocarbons[16] and CO$_2$[17,18] with ILs. Differently from all of them, the present review focuses stringently on the high-pressure application, critically surveying the literature from this perspective. As follows, the reader will find a short overview on the most important IL properties for successful separation/electrocatalysis at high pressure (cf. section Ionic Liquids in brief); the principles guiding the IL molecular tuning (cf. section Design principles for ILs), and their correlation with the CO$_2$ solubility diagram at high pressure (cf. section The CO$_2$-IL interactions into details); a survey on the few physically measured solubilities at high pressure (cf. section High-pressure CO$_2$ and CH$_4$ solubilities in ILs); current advances in IL-based separation technologies (cf. section High-pressure processes for CO$_2$ separation employing ILs), and, finally, the promising use of ILs for further CO$_2$ processes via electrocatalysis, which may potentially serve for IL-regeneration (cf. sectionCO$_2$ (Eletro)catalysis either in IL or at High-pressures).

Ionic Liquids in Brief

Molecular perspective.—Ionic liquids (ILs) are usually defined as compounds formed solely by ions with a melting point below $T =$ 100 °C.[19] They are usually composed of large organic-based ions linked by well-balanced Coulomb bonds and charge dispersion interactions. These strong and stable ionic interactions partially explain their high thermal stability and their negligible vapor pressure.[20] In general, ILs present negligible vapor pressures at temperatures below 100 °C. However, the myth that the ionic liquids were not volatile was only broken in 2006, when Earle & coworkers showed that some aprotic ionic liquids could be distilled at 200 °C–300 °C at low pressure of 10^{-4} bar, with simultaneous recovery of significant amounts of pure substance.[21] Corroborating this remarkable piece of evidence is recent theoretical insights based
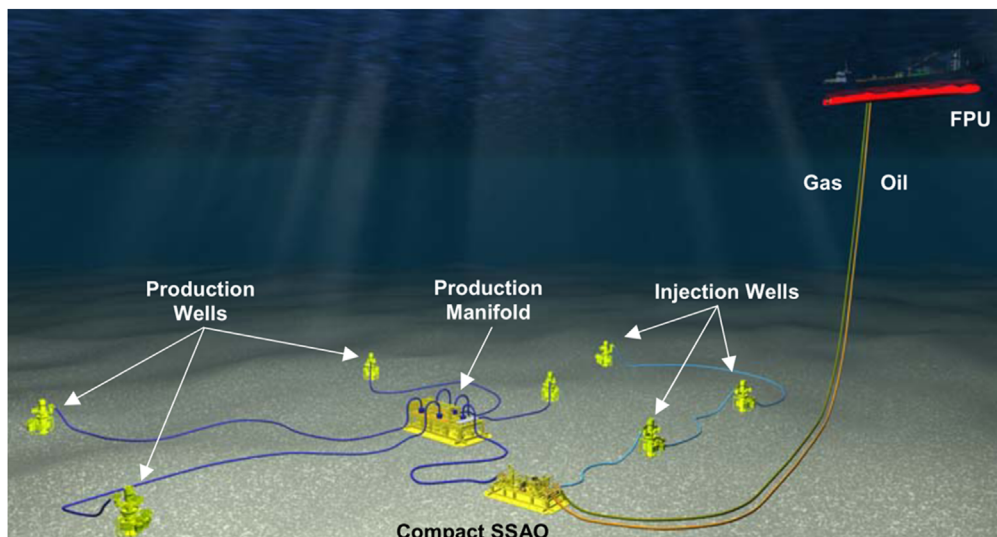
Figure 1. Scheme of subsea separation unit. FPU is an acronym for floating process unit. On the seafloor lays a compact SSAO that is an acronym in Portuguese for "separação submarina água-oleo" or subsea water-oil separation unit. Currently, the CH_4/CO_2 separation is made on the FPU. Reprinted with permission from "Albuquerque et al. in *Offshore Technology Conference*, Houston, Texas, USA, 2013"[3]—Copyright Offshore Technology Conference.

on predictive methods, which found the equilibrium vapor pressure 10^{-5} bar at 30 °C for a broad IL variety.[22–24] Further, the large ions promote an easier charge dispersion and hamper the formation of crystalline structures, resulting in lower fusion temperature substances.

In general, all ILs are reported in abbreviation forms like [C4mim][PF$_6$], which represents the species formed by the butyl-methyl-imidazolium [C4mim]$^+$ cation and by the hexafluoro-phosphate [PF$_6$]$^-$ anion. Figure 2 exhibits both the chemical structure and the inducted charge dispersion of the standing-alone ions for typical IL ions alongside two other monoatomic ions. Besides, Fig. 2 also shows the structure for other ions like [Pyrr]$^+$ and [But]$^-$ to illustrate how the inducted charge dispersion varies with the IL-ion chemical structure. All the chemical structures were pre-optimized by MMFF94 force field via AVOGADRO *software*, whereas the induced charges were estimated through the Hartree-Fock and TZVP basis set level of theory via the GAMESS *software*, and finally the visual display of each ion-induced charges produced via JCOSMO *software*, as described elsewhere.[25] The negatively induced charges on the vicinity of [C4mim]$^+$ are represented by the blue color scale. Similarly, the positively induced charges are represented by a red scale on the vicinity of [PF$_6$]$^-$ anion. As noted, the induced charges are spatially dispersed through the carbonic chain of the IL's ions, which in turn, uniforms the ion's charge density and potentially reduces the strength of local ionic interaction. The large size of IL ions together with their spatially distributed induced charge hamper the formation of crystalline structure, resulting in ionic species with low fusion temperature in comparison with the smaller monoatomic ions, such as Na$^+$ and Cl$^-$.

ILs can be categorized through several metrics, such as their fusion temperature, number and types of ions, the existence of task-specific groups, and the nature of their ionic interaction. The latter can be tuned by going from aprotic (AIL) to protic ionic liquids (PIL).[26] The latter predominantly form their ionic interaction through a proton donation, which is less stable than the aprotic interactions. AILs usually present higher thermal stabilities,[27,28] lower vapor pressure, and more complex synthesizing routes than PILs. Imidazolium- and pyridinium-based cations are the most usual structure of AILs ions chosen to be investigated.[8] PILs are usually less expensive, easier to be synthesized, and more environmentally friendly[29] than common AILs, and usually present lower thermal stability[30] and lower conductivity[31] when compared with AILs. Nevertheless, both types of IL presented a high absorption of CO_2[8,9] and low absorption of CH_4, leading to high CO_2 selectivity.[9–11]
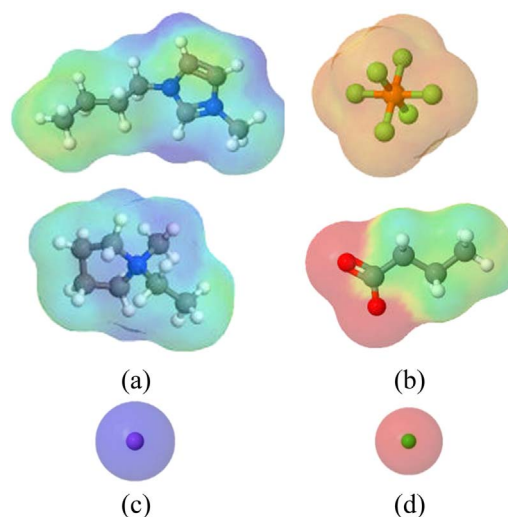
Figure 2. Chemical structure and inducted charge dispersion for two typical IL anions (a) [C4mim]$^+$ and [Pyrr] $^+$; cations (b) [PF$_6$]$^-$ and [But]$^-$ together with two monoatomic ions (c) [Na]$^+$ and (d) [Cl]$^-$. The JCOSMO software assisted in the image creation.
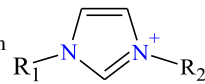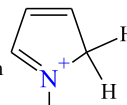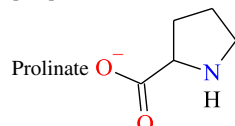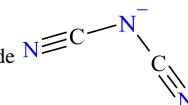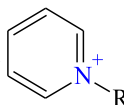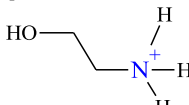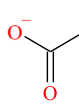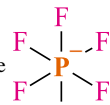
Some of the common ions used in CO_2 capture can be observed in Table I. In fact, there are myriad possibilities to combine a cation and an anion to obtain an ionic liquid suitable to capture CO_2. However, the understanding of molecular interaction between ILs and CO_2 is an essential issue to design such combinations. Therefore, many efforts have been devoted to characterizing the molecular interaction of CO_2 with different cation and anions.[27,32,33]

Properties.— *Viscosity (η).*—Depending on its application, the IL viscosity would be its worst disadvantage. The strong ion-ion interactions and large molecular size result in overall high viscosities. This might reduce mass transfer rates and increase the pressure drop along with the fluid transport through the pipes.

Figure 3 shows comparatively viscosities measured in neat ILs at $T = 25$ °C and $P = 1$ bar.[31,34–41] Despite overall high viscosities presented by most ILs, many others can present significantly lower values, but still higher than water, except by [DEA][Bu]. The crude-oil transport in pipelines is economically viable only for viscosities

Table I. Typical ion structure of ILs used in CO$_2$ capture processes.

Cation Structure		Anion Structure	
$[R_1R_2Im]^+$ Imidazolium	$[Pyrr]^+$ Pyrrolium	$[Pro]^-$ Prolinate	[DCA] Dicyanamide
$[Py]^+$ Pyridinium	$[2HEA]^+$ or $[HEA]^+$ 2-Ethylammonium	$[Ac]^-$ Acetate	$[PF_6]^-$ Hexafluorophosphate

below 500 mPa·s^{-1}.[42] As noted, the viscosity of some ILs is well above the required level for pumping, being those gather aside on the top scale in Fig. 3 together with glycerol viscosity. Among the ILs presenting suitable viscosities for pipeline transportation, those presenting viscosities below 200 mPa·s^{-1} correspond to the most cost-effective alternative for fluid transportation by oil pipelines. The olive oil is gathered together with those ILs presenting the lowest viscosities for cost-effective transportation.

When in presence of a CO$_2$-rich atmosphere, the IL viscosity modifies due to the CO$_2$ dissolution into ILs. As a representative of macromolecules, the long-chain-ions-containing ILs exhibit mechanical behavior intriguingly similar to aliphatic polymers, i.e. the dissolution of short molecules promote smaller inner friction among the contacts of different atomic centers among the macromolecule, which for aliphatic polymers causes a reduction in viscosity; those short molecules are additives named plasticizers. By analogy, the CO$_2$ dissolution into ILs plays the role of plasticizer. For those ILs for which CO$_2$ plays the role of plasticizers, the CO$_2$-IL interaction may be said to be governed by the CO$_2$ occupation into the IL inner free volume. Yet if otherwise, the CO$_2$ dissolutions in IL do not vary or even induce an increase of the IL viscosity, the CO$_2$-IL interaction may be said to be governed by chemical CO$_2$ interaction with the IL functional groups. Regarding the water content, it promotes a reduction of the water-rich IL viscosity, except for small water contents that can increase it.[40]

Intrinsic ionic conductivity (Λ).—Like any other dielectric medium, ultrapure water only attains substantial ionic conductivity if "contaminated" with molar tenths of external ions that promptly get solvated by water molecules, passing to act as a fundamental unit of charge transportation, i.e., charge carrier. Contrariwise, neat ionic liquids exhibit an intrinsic ionic conductivity that overall lays below 30×10^{-3} s·cm^{-1}. Such intrinsic conductivity can be attributed to the degree of ionicity in its pure form. Nevertheless, only a mild improvement on the ionic conductivity is attained with the addition of monoatomic ions, which strongly indicates viscosity imposes a substantial friction action over the motion of the ions. For instance, [C2mim][FSA] reaches at best 70×10^{-3} s·cm^{-1} when the monoatomic cation like sodium replace 50% of the IL-cations,[43] being a negligible improvement in comparison to water that elevates the ionic conduction from 6×10^{-8} s·cm^{-1} for ultrapure-water to 800×10^{-3} s·cm^{-1} for 0.1 M of aqueous KCl solution. The foundations to understand the important role played by both the IL viscosity and ionicity on IL intrinsic ionic conductivity are discussed below.

The impact of IL viscosity on its intrinsic ionic conductivity has been discussed on the basis of Walden's original observation of organic electrolytes.[44] The molar conductivity (Λ_m) correlates to the fluidity of the medium through which the ions move (represented by the inverse of the viscosity, η^{-1}); so that, it is expressed by the Walden Rule: $\Lambda_m \cdot \eta^{-1} =$ constant. On a plot of log Λ_m vs log η^{-1},

this rule predicts a straight line, and the plot has become known as a "Walden plot." This plot demands the molar conductivity Λ_m (S·cm^{-2}·mol^{-1}) defined as $\Lambda_m = \Lambda \cdot V_E^{-1}$, where Λ (S·cm^{-1}) stands for the conductivity measured by the electrochemical impedance spectroscopy and written as Λ_{imp} or Λ_{EIS}; and, V_E stands for the volume containing one Faraday of positive charge. The experimental density (ρ), which in this case is a function of temperature, demands to be known for V_E to be calculated by $V_E = \rho \cdot M_w^{-1}$, where M_w is the IL molar mass.[45] Data from a wide range of electrolytes can then be placed on the Walden plot, including any ionic liquid for which viscosity, conductivity, and density measurements are available. When this data set can be carried out over a broad temperature range, their representation on the Walden plot interestingly follows a straight line as those seen in Fig. 4. If otherwise, only a single temperature had been exploited, only a single point would be displayed on the Walden plot for each IL, as shown by Zhao et al.[39]

Figure 4 shows the Walden plot for a few ILs tested in electrochemical applications.[39,47,50–53] Rather than covering the literature extensively, this review curbs the core topics about IL conductivity, offering a broad picture of the issue. The linearity of the experimental data indicates Walden Rule is obeyed so that the ILs can be interpreted similarly to the aqueous KCl solutions at high dilution. The solvated ions in aqueous media are known to be fully dissociated and have to have equal mobility. In this context, the conduction for 0.001 M aqueous KCL is taken as a reference. Its value at room conditions is represented by a symbol of star in the plot (a) in Fig. 4, while the lines are just an extension of the Walden role, $\Lambda_m \cdot \eta^{-1} =$ constant. The same is valid for lines traced for higher KCl concentrations. The Walden plot had been extensively discussed by Angell & coworkers[45,49,54] that suggested using the Walden plot for a general classification of ILs. Except for one or two notable exceptions,[45,49] most ionic liquids fall below the ideal lines, more or less so depending on their structure. According to Angell & coworkers, the ILs that fall below the ideal line for 0.001 M KCl in the Walden plot are classified as poor ionic conductors or even non-conductors, as does [C2mim][BF4][46] in Fig. 4. Still, according to Angell & coworkers, the ILs with conductivity above the ideal line (1 M KCl) are classified as superionic conductors, as the [DEA][HSO4]. For this IL, two points are displayed in the graph; both estimated by Zhao et al. 2008,[39] while one point used the upper limit of viscosity from equipment used by the authors, the other considered a viscosity ten times higher. Despite such imprecision, the [DEA][HSO$_4$] still lays within the superionic ILs zone. Furthermore, it should not be of interest for electrocatalysis due to the low mass transport rates (product/reactant) imposed by its high viscosity; even though, it can be of potential interest for batteries.

The empirical rule of Walden matches theoretical grounds when interpreted in light of the theory-derived equations, namely the Stokes-Einstein and Nernst-Einstein equations. In both the models, ions are approximated to hard spheres. Although moving at the action of different force fields (the mass and electrical fields,
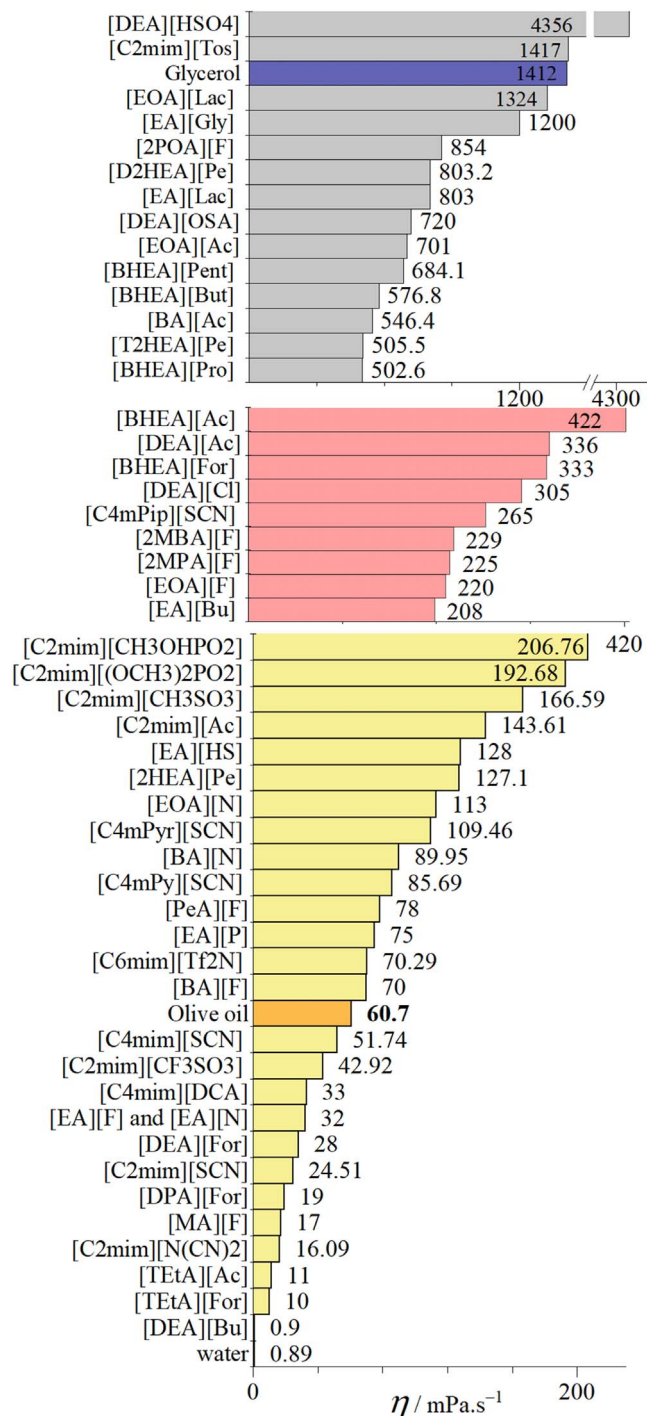
Figure 3. Dynamic viscosities (v) of 48 ionic liquids measured at $T = 298.15$ K and $P = 1$ bar by different authors as Zhao et al. 2000[8],[39] Chennuri & Gardas 2016,[36] Iglesias et al. 2010,[38] Widegren & Magee 2007,[31] Greaves et al. 2006,[41] Xu 2013,[35] Domanska & Królikowska 2012,[37] Alcantara et al. 2018[40] and Freire 2011.[34] The viscosities of water, olive oil and glycerol are also shown for getting IL-viscosities into perspective.

respectively), they are subjected to very similar counteraction forces. The friction imposed by hydrodynamic displacement of the forward fluidic medium is of similar nature for both cases. In particular, the Stokes-Einstein model takes explicitly into consideration the fluid viscous forces as the counteraction friction, and then the ionic diffusion of specie i (D_i) is related to the medium viscosity η through the Stokes-Einstein equation

$$D_i = \frac{k_B T}{C}\left(\frac{1}{s_i}\right)\eta^{-1} \qquad [1]$$

where T is the temperature, η is the bulk viscosity of IL, K_B is the Boltzmann constant, s_i is the Stokes radius of the ion (s_+ for cation and s_- for anion), and C is a constant based on the slip ($C = 4\pi$) or stick ($C = 6\pi$) boundary condition. When the ions in question are the own constituents of the viscous medium, coefficient D_i is named self-diffusion coefficient. Alternatively, the Nernst-Einstein model correlates the ion self-diffusion coefficients of both cations ($D+$) and anions ($D–$) with the molar conductivity ($\Lambda_m \rightarrow \Lambda_{NE}$)

$$\Lambda_{NE} = \frac{N_A e^2}{k_B T}(z_+^2 D_+ + z_-^2 D_-) \qquad [2]$$

where k_B is the Boltzmann constant, N_A is Avogadro's number, e is the charge of an electron, T is the absolute temperature, and $z+$ and $z—$are the cation and anion charges. If accurately stoked to the original models, the ion diffusion coefficients on the Nernst-Einstein model would be instead defined as the ion mobility. However, in the context of IL conductivity, the self-diffusion coefficient, D_i, can be approximated to the ion mobility ($D_i \rightarrow D_+ or D_-$), thus resulting in the combined equation.

$$\Lambda_{NE} = \frac{N_A e^2}{C}\left(z_+^2\left(\frac{1}{s_+}\right) + z_-^2\left(\frac{1}{s_-}\right)\right)\eta^{-1} \qquad [3]$$

Such a combined equation gives the theoretical foundation to interpret the empirical Walden's role on a molecular level. Despite the Stokes-Einstein equation being most appropriate for the case of large ions moving in a solvent of small molecules, we will see here that the Walden rule applies, rather well, to pure ionic liquids. MacFarlane et al.[55] demonstrated that the combined equation (Eq. 3) adjusts quite well to the experimental data, which in turn could justify, although in part, the vertical displacement on the Walden plot seen for the ILs in relation to the line traced by "ideal" KCl aqueous solution. Following the arguments of MacFarlane et al., small vertical displacement in relation to 0.001 M KCl solution on the Walden plot seen in Fig. 4 for [C2mim][BF4] could be justified by the Stokes radii of the ions (s_i), i.e., the radii differences between the cations K^+ and $[C2mim]^+$ and between the anions Cl^- and $[BF4]^-$. Still, according to this rationale, the neat [C2mim][BF4] would have a similar ionicity of 0.01 M KCl solution.; however, an overall conductivity is reduced due to the larger radii of both $[C2mim]^+$ and $[BF4]^-$. At this point, the concept of ionicity of ILs has to be evoked.

The ionicity (I) can be quantified either by comparing self-diffusion coefficients (D_+) or by comparing the molar conductivities (Λ_m), either of which measured with different techniques. On the one hand, the indirect approach estimates D_+ ($D_+ \rightarrow D_{imp}$) by considering conductivity measured with the electrochemical impedance at high frequency ($\Lambda_m \rightarrow \Lambda_{imp}$) into the Stokes-Einstein/Nernst-Einstein combined equation, cf Eq. 3. On the other hand, the pulsed field gradient NMR (PFG-NMR) technique is a straightforward approach to measure the self-diffusion coefficients ($D_+ \rightarrow D_{NMR}$), once it detects the motion of atomic nuclei like Hydrogen or Fluor. Alternatively, the molar conductivity ($\Lambda_m \rightarrow \Lambda_{NMR}$) can be estimated from the self-diffusion coefficient (D_{NMR}) experimentally measured with the PFG-NMR and, then, compared with Λ_{imp}. In either case, the ionicity can be experimentally defined as

$$I \equiv \frac{\Lambda_{imp}}{\Lambda_{NMR}} \text{or } I \equiv \frac{D_{imp}}{D_{NMR}}. \qquad [4]$$

There is an important number of works in the literature describing this approach to evaluate the ionic conductivity of different types of
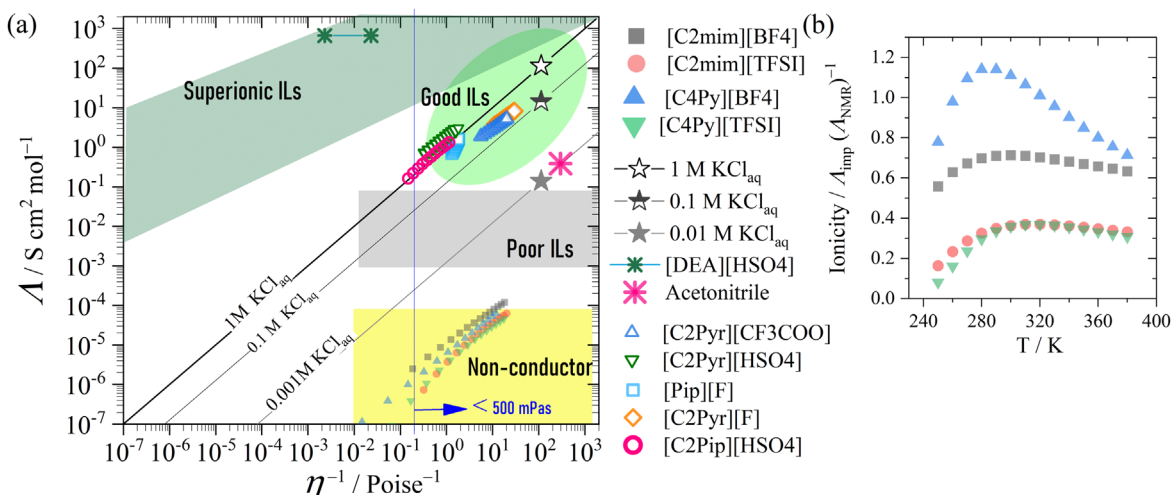
Figure 4. The Walden plot for a few ILs tested in electrochemical applications (a) and their respective ionicity (b). The data was generated with the adjusted model to the experimental data (density, conductivity, and viscosity) obtained by Noda et al. 2001,[46] Zhao et al. 2008,[39] Wu et al. 2010[47] and Chapter 7 in the Handbook of Reference Electrodes.[48] Plate b display data exclusively from Noda et al. Vertical line in the plate (a) indicates the viscosity at 500 mPa s. The highlights in plate (a) follow the classification proposed by Angell & coworkers.[49] Acetonitrile used 0.1 M [NBu4]ClO4 at 295 K.

ionic liquids.[56–62] According to Watanabe & co-workers,[63] the degree of ionicity or $\Lambda_{imp} \cdot (\Lambda_{NMR})^{-1}$ values, as seen in Fig. 4b for PILs, plays role in the ionic conductivity, exhibiting an excellent correlation with coordinating abilities of the cations and the anions and/or the overall interactions in the ILs under chemical equilibria. Recently, Nordness & Brennecke[64] extended the ion dissociation analysis for a broad range of ILs and IL solutions (aqueous and nonaqueous). However, without hydrogen or fluor atoms within the ion structure, it is unfeasible to employ the PFG-NMR technique. In those cases, the ionicity is impossible to be measured via experiments, even though the combined Stokes-Einstein/Nerst-Einstein equation offers a good approximation to obtain the values of ion diffusion.

A broad picture of the IL physical behavior has been scrutinized by Angell & co-workers,[45,49,54] being a few of their insights commented here but in the context of selecting an IL for electrochemistry. Walden plot in Fig. 4 explicitly shows the IL-viscosity issue related to its intrinsic ionic conduction. As said repeatedly, the viscosity of 500 mPa·s is the target mark below which pumping from the seafloor to sea surface is profitable at the industrial level; thus, 500 mPa· is also the benchmark for electrosynthesis/electrochemistry. As seen in Fig. 4, despite all ILs to attain viscosity below 500 mPa·s, only a few display suitable conduction for operating in an electrochemical cell, being those highlighted in green. Alternatively, an intrinsically poor ionic conductor may be mitigated by adding monoatomic ions such as Na + (supporting electrolyte); however, it seems not to be a good strategy in this case, otherwise indispensable.

An underlying justification between the good and poor IL-conduction in Fig. 4 were first formulated by both MacFarlane et al. & Angell et al., and latterly complemented by Paluch et al. In general lines, it was proposed two conductivity mechanisms, Grotthuss (proton hopping) and vehicle (molecular transport) mechanisms. The vehicle mechanism tends to be more dominant when the temperatures are far above the IL temperature of glass transition (T_g). If, otherwise, the IL tends to be "parked" in face of the electrical field because both the forward and backward motions occur almost at the same frequency. As result, there is motionless in translational terms, which is said to be a cooling state; thus, the vehicle mechanism tends to contribute to the overall conduction lesser and lesser, the nearest the temperature is to T_g. If no other mechanism of conduction is present, the tends to have poor intrinsic conduction as represented by the imidazolium-based ILs in Fig. 4a, to which the room temperature is far above both the T_g (around −100 °C). Contrariwise, a few PILs are capable of retaining a high

ionic conductivity despite temperature nearing their T_g, and Fig. 4a depicts this case for [DEA][HSO4], to which the room temperature is less distant to T_g (around −65 °C) than aforementioned ILs. In this context, Paluch et al.[65] propose the conductivity transitioned from a vehicle to a Grotthuss mechanism. Despite the (super)cooling state, the proton being a small specie can easily transit from one ion to another due to the action of the electrical field by overcoming the local potential barrier for proton jumping two vicinal anions, which renders a high proton conductivity offer observed in some viscous PILs. It is worth to be mentioned that [DEA][HSO4] although highly conductive is unsuitable for application in electrosynthesis.

According to the vehicle mechanism, the charge transport occurs through the displacement of molecular obstacles by the ion carrying the charge; also following the Stokes-Einstein equation (Eq. 1). At the Walden plot (Fig. 4), the ILs that exhibit predominantly this mechanism can be observed somewhere on or below the "ideal" (1 M of KCl aqueous solution). Furthermore, for the ILs plotted far below this line, their ionic conductivities cannot be solely attributed to differences in their viscosities. Previous studies reported that IL ionicity can promote changes in ionic conduction.[66] However, their ionicity cannot be easily predictable given the several possible interionic interactions (i.e. Coulomb forces, dispersive interactions, $\pi...\pi$ stacking, hydrogen bonding, etc.). According to the Grotthuss mechanism, the superionic IL region is located above the 1 M "ideal" line on the Walden plot and features electrolytes with high ionic conductivity due to the proton hopping mechanism and low viscosity due to the "supercooled" effect (near to T_g).

Thermal physical properties.—Ionic liquids are often claimed to be thermally stable because of their very high decomposition temperature (T_d). For ammonium- and imidazolium-based ionic liquids, T_d can reach as large values as 470 °C, when considering thermogravimetric analysis (TGA) in the mode of ramped temperature.[28] Instead, Maton et al.[28] suggested that more accurate T_d values would be measured if used a fixed temperature protocol. In this mode, an isothermal TGA has to be measured over a prolonged and fixed time, for instance, 2, 15, or 20 h, and the time frame which allowed 10% weight loss defined as the accurate T_d. According to this protocol, ionic liquids can reach 393 °C as the highest T_d among the ammonium- and imidazolium-based ILs tested by the authors. In pragmatic terms, the thermal stability of the fluidic phase is marked by the interval between the melting temperature (T_m) and decomposition temperatures (T_d). Most ionic liquids exhibit wide ranges of thermal stability, around 100 to 200 °C.[27]

Interestingly, the high-pressure CO_2 has a substantial effect on the IL melting point as compared to the atmospheric-pressure CO_2. Such a melting point depression can reach a dramatic value of 120 °C. Serbanovica et al.[67] presented meticulous experiments on high-pressure CO_2-induced melting point depression. The authors elucidated that the nature of the anion and its interaction with the CO_2 molecule seems to have a predominant influence on the melting behavior, while the cation seems to play a role of either hindering or allowing that interaction.

Besides, the ILs exhibits a second-order phase transition known as the glass transition temperature (T_g) that can be correlated with many other IL physical-chemical properties such as conductivity, heat capacity, and melting point. Pitawala et al.[68] showed that the length of the alkyl chain on the cation has no, or a weak, influence on the T_g whereas the presence of rigid aromatic side groups has a strong influence in increasing T_g. The highest ionic conductivity is 59×10^{-3} s·cm^{-1} at 25 °C for an ionic liquid with a decane chain and one methyl group on each imidazolium ring. Other properties, such as the heat capacity and melting point, also change associated with T_g.[69]

Design Principles for ILs

There are several ways of combining ions to tune the IL's physical-chemical properties. The present section summarizes the latest strategies used to design IL-ions to obtain higher CO_2 absorption capacities at atmosphere pressure, one of the most intensively tackled IL properties over the years.

Blends/hybrid solvents.—The physical mixture of different classes of CO_2-absorbers can be used to regulate specific IL properties.[70–73] Two examples of how to regulate IL properties are presented here. In the first example, amines and ILs can be mixed together into an aqueous solution mostly aiming at optimizing CO_2 solubility for a low-viscosity aqueous-based solvent. In the 2.5 molal of 1-butyl-3-methyl-imidazolium acetate, [C4mim][Ac], CO_2 solubility reaches 0.005 mol of CO_2 per mol of [C4mim][Ac] at $T =$ 30 °C and $P \sim 21$ bar. Twice as larger CO_2 solubility can be reached with bends. In 2.5 molal of [C4mim][Ac] blended with 0.5 molal of 1-(2-aminoethyl) piperazine (AEP), CO_2 solubility reaches 0.013 mol of CO_2 per mol of [C4mim][Ac]/AEP at $T = 30$ °C and $P \sim 21$ bar.[70] The incorporation of reactive and volatile alkanolamine molecules within the stable ionic liquid structures can produce protic ILs (PILs) with moderate thermal stability,[30,74] low toxicity,[29] and moderate to high CO_2 solubility.[34,75] Despite presenting lower CO_2/CH_4 selectivity[76,77] than their original alkanolamine structures,[5,78] these PILs still present high CO_2/CH_4 selectivity compared with other physical CO_2-absorption ILs.[76,77] Infra-red spectroscopy and ^{1}H/^{13}C NMR studies indicate that these ILs and CO_2 interaction mechanisms could be tuned from chemical interactions[79,80] to physical interactions,[11,40] depending on the IL structure.

In the second example, macromolecules are mixed with pure IL aiming at reducing the overall solvent-based cost. For instance, the ionic liquid butyl-trimethyl-ammonium bis(trifluoromethylsulfonyl) imide, [N4111][NTf2], and the macromolecule poly(ethylene oxide), PEO1000, mixed in molar ratio 0.25 to 0.75 exhibits CO_2 solubility of 0.22 mol of CO_2 per mol of blend at $T = 50$ °C and $P = 5$ bar against 0.12 mol and 0.26 of CO_2 per mol of pure [N4111][NTf2] and pure PEO1000, respectively.[73]

Deep eutectic solvents (DES).—In 2001, Abbott et al.[81] demonstrated the synthesis of conducting materials that were viscous liquids at or around room temperature, insensitive to moisture, and much cheaper than imidazolium-based liquids. The material obtained by heating organic quaternary ammonium chloride and inorganic chloride presented an impressive decrease in the freezing points, from hundreds of Celsius degrees, typical for the ammonium-based chloride to mild tens Celsius degrees for the final viscous

material. Abbott et al. had also extended the concept over choline chloride/urea[82] and choline chloride/carboxylic acids,[83] naming the mixture as a deep eutectic solvent (DES).

DESs are a homogeneous and eutectic (i.e. they present lower freezing temperature than the pure components) mixture between salt and a complexing agent (CA).[84] Typically, the CA acts as a hydrogen bond donor (HBD) whereas the salt acts as a hydrogen bond acceptor (HBA).[14,85–87] Among the most employed HBDs are urea, glycerol, ethylene glycol, and amino acids whereas choline chloride (2-Hydroxyethyl-trimethylammonium) have been the most ordinarily used HBA. For CO_2 capture, choline chloride/urea (named as reline) has been the most investigated DES,[17,88] exhibiting CO_2 solubility of 0.399 mol of CO_2 per mol of DES at $T = 70$ °C and $P = 63.5$ bar.[17] Haider et al.[89] studied choline chloride and ethylene glycol as DES and obtained solubility of 0.06 mol of CO_2 per mol of DES at $T = 30$ °C and $P = 15$ bar.

Within the last five years, renewed interest in DESs for CO_2 capture has led to the exploration of new compositions.[84,89–91] In order to obtain DESs with new compositions, the concept of DES synthesis was widened. Now, HBD is considered to be a Lewis base, and HBA, a Lewis acid. With this renewed concept, the IL cation could take over the HBD rule, whereas the IL anion, over the HBA rule. According to this rationale, Yan et al.[91] selected a superbase IL to synthesize a DES with improved CO_2 absorption. The authors employed [HDBU][Im] as superbase-IL and viscous ethylene glycol (EG) as Lewis acid and found that the resulting DES (ratio IL:EG of 7:3) was capable of absorbing 0.141 grams of CO_2 per grams of DES at $T = 313$ K and $P = 1$ bar, which corresponds to ~0.4067 moles of CO_2 per mol of DES or yet ~0.9613 mol of CO_2 per mol of DES if considering the IL content alone. Interestingly, the same authors reported that such DES was capable of fully releasing the absorbed CO_2 at $T = 343$ K by simply purging N_2 throughout the DES, and the overall CO_2 absorption capacity remained at the same value even at a few capture/regeneration cycles.

Employing the same rationale, Zhang et al.[86] obtained a maximum of ~1.0 mole of CO_2 per mol of DES and the kinetic of absorption was tuned by the molar ratio HBA to HBD. The authors used mixtures of [Bmim][Cl] and imidazole (Im) at different molar ratios as IL and 1,5-diazabicyclo [4.3.0] non-5-ene (DBN) as superbase. Haider et al.[90] reported 0.29 mol of CO_2 per mol of DES at $T = 313$ K and $P = 10$ bar for a mixture of tetrabutyl ammonium bromide (TBAB) mixture and methyldiethanol amine (MDEA), being the HBD role played by MDEA.

Task-specific Ionic liquids (TSIL).— *Amino-functionalized IL.*— Davis et al.[92] proved the concept of IL functionalization. Their main objective was to improve the CO_2 solubility at atmospheric pressure. The authors synthesized an IL similar to the one used by Brennecke et al.,[6,8] who demonstrated the IL capability of high CO_2 solubilities at high pressure by the first time. For achieving these solubilities, functionalized cations were used, i.e. an amino group was inserted in the cation [bmim]. Whereas the [bmim][BF$_4$] used by Brennecke et al. reported negligible CO_2 solubility at $T = 30$ °C and $P = 1$ bar, Davis et al. reported 0.5 mol of CO_2 per mol of [Apbim][BF$_4$] in the same conditions. Later on, Zhang et al.[93] proved that a dual amino-functionalized cation would lead to a twice as larger solubility, i.e. 1.05 mol of CO_2 per mol of IL at $T = 30$ °C and $P = 1$ bar.

Since then, one or two amino-functionalized cations[94,95] and anions[96–103] have been synthesized and investigated. Experimental measurements of CO_2 solubility,[33,104] spectroscopic investigations,[33,104] and numerical simulations[33] indicate that the CO_2 solubility in imidazolium-based IL depends essentially on the nature of the anion, being the cation a secondary player. Recently, this conception was contested by Hollóczki et al.[105] who advocated that significant attractive interactions exist between the cations π-bonds and the CO_2 in ILs containing imidazolium-ring.

Amino-acids-functionalized IL.—For anions of amino acids, the further addition of amino acid groups increases the capacity of CO_2

absorption. For instance, Yang et al.[97] observed ca. 1.0 mol of CO_2 per mol of IL when the IL structure has an amino group bound to the rigid carbon-based ring that creates an electrostatic environment that prevents the deprotonation of the carbamate group. When two carboxyl groups are incorporated in the anion of the IL ca. 1.69 mol of CO_2 per mol of IL can be reached.[106] Figure 5 sketches the multiple-absorption chemical-sites mechanism of CO_2 capture by multiple amino-acids-functionalized ILs.

Ester- and ether-functionalized IL.—Ester- and ether-functionalized ILs have been developed to obtain better CO_2-selective ILs, besides reducing both IL toxicity[107] and viscosity.[108,109] For instance, the use of ether-functionalized cations, in particular phosphonium cation that contains a methoxy group, exhibited quite low viscosities at $T = 25$ ºC, ca. $\upsilon = 35$ and $\upsilon = 44$ mPa·s, and quite high thermal stability, i.e. up to nearly $T = 400$ ºC.[109] Regarding CO_2 selectivity, Bara et al.,[107] synthetized ether-functionalized imidazolium cations based on oligo(ethylene glycol) functional group substitutes in the lateral chain of the imidazolium cation. This imidazolium TF_2N ionic liquid, which is ether functionalized, exhibited CO_2/CH_4 ideal selective solubility of 30%–75%, higher than its corresponding alkyl analogues. A similar trend was reported by Deng et al.[110] and Zhou et al.[111] Kanakubo et al.[112] extended the ether-functionalized ion concept over the anion and noted an improvement in the CO_2 solubility at high pressure. Regarding the ability of ester and ether functional groups to modulate the intermolecular interaction with CO_2, it was suggested that the oxygen atom in the ether group (a Lewis base) interacts with the carbon atom on the CO_2 molecule (a Lewis acid) forming a Van der Wals complex.[113]

Regulating the ion basicity.—In 2010, Wang et al.[114] synthetized a bunch of the so-called super-base ILs by simply mixing a super-base with a weak acid. In this mixture, the super-base has the ability to deprotonate weak proton donors, such as phenol and imidazole. Such liquids present low viscosity, low melting point, and CO_2 absorption capacity around or even higher than 1.0 mol of CO_2 per mol of IL. Li et al.[115] observed that the choline cation, which is a superbase cation, combined with different anions always results in an absorption greater than 1.0 mol of CO_2 per mol of IL at 25 °C and 1 bar.

Wang et al.[116] categorically proved that the capacity of CO_2 absorption positively and linearly correlates with both the Azole (nitrogen hetero-ring) anion pKa and the absorption enthalpy. Additionally, the authors reported a negligible variation in the IL's viscosity with the CO_2 absorption, which in turn, corroborates with the fast kinetic rates of CO_2 absorption. Since then, the IL basicity became an important criterion for designing ILs with either better CO_2 absorption capacities or lower absorption enthalpy, which can save energy during the IL-regeneration process. The presence of water in super-base ILs favors the CO_2 absorption capacities.[117] In this regard, Zanatta et al.[118] propose a mechanism of CO_2 absorption/desorption assisted by water for super-base IL.

Internal free volume (IFV).—Interestingly, the glass transition temperature (T_g) is not the only characteristic in common for ILs and polymers. Both also exhibit substantial variations on the molar volume under the dissolution of a small-molecule solute into their bulk, which is an indication of small, if not negligible, volume expansion. For ILs, this effect was first noted by Blanchard et al.,[8] who noted a linear correlation between CO_2 solubility and pressure, which suggests a space-filling mechanism of CO_2 absorption. In the review of Zeng et al.,[14] the reader finds a compressive survey on the most exciting advances on this topic.

The CO₂–IL Interactions Into Details

The nature of the chemical interaction between IL-molecules and $scCO_2$ can be directly inferred by experiments employing spectroscopic methods, such as in situ Attenuated Total Reflection Infrared Spectroscopy (ATR)[119,120] and in situ NMR spectroscopy.[32,121–126] In fact, there was a significant evolution in the understanding of CO_2–IL molecular interaction when these techniques were used under high pressure. For instance, one of the best examples of the application of high-pressure NMR spectroscopy to elucidate the interaction of CO_2 with imidazolium ionic liquids was brought by Corvo et al.[32] These authors observed that the IL structure is not greatly affected by the solvation of CO_2, which occurs without disrupting the cation-anion hydrogen bonds. In turn, suggesting that CO_2 is not competing with the anion for the same locations in relation to the cation because it is establishing weaker interactions. More recently, the same authors[122] used different NMR experiments to quantify CO_2 sorption and to evaluate the interaction between PIL/IL−CO_2PIL@IL composites. Their results show the possibility to control the sorption pathway according to the PIL/IL ratio, ions structure, and water amount. Moreover, their results also suggested that the 3D organization of PIL composites was similar to native ILs. In situ ATR was also used under high pressure to characterize the molecular interaction between ILs and CO_2. For instance, Seki and co[120] used this technique to elucidate the molecular interactions between dissolved CO_2 and three different imidazolium-based room-temperature ionic liquids that are swollen under $scCO_2$ conditions. Their results show that both cation and anion species impacted the molecular state of the dissolved CO_2 due to the Lewis acid-base interaction. Nevertheless, these strong Lewis acid-base had no effect on the solubility of CO_2 in this type of ILs was governed either by the affinity of CO_2 for fluorine atoms or by the IL-free volume. Albeit successful, these in situ approaches require sophisticated, cost-intensive experimental apparatus that justifies their unspreaded use worldwide and limits the advances their employment could produce. In this context, the next subsections will be focused on more traditional approaches to inferring physical-chemical adsorption of CO_2 in ILs, such as phase equilibrium,[8] IL-molar volumes,[127] and CO_2 absorption enthalpy.[128]

Physical CO₂ absorption in ILs.— *Brief theory.*—The physical interaction mechanism between ILs and CO_2 has been mostly deciphered by means of theoretical approaches. Among the published models, the empty space theory[129] is arguably one of the most accepted ones. In summary, an empirical correlation was observed between the inter-ion empty spaces and the amount of CO_2 dissolved in the ILs. Thus, ILs with large and less polar ions promote weaker ion-ion interactions; therefore, generating larger empty voids and greater CO_2 solubility. However, large empty spaces can also promote the solubilization of other larger molecules, such as those of light fuel gases. Thus, according to this theory, the ILs CO_2
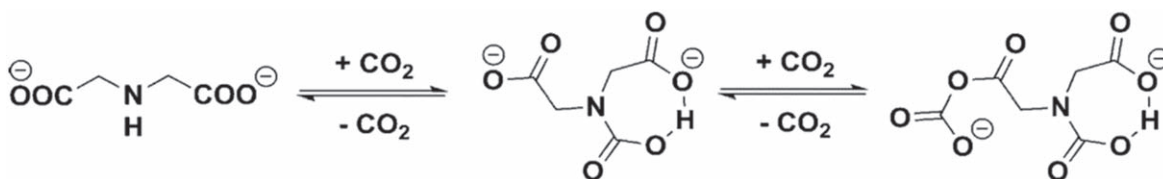
Figure 5. Interaction mechanism of CO_2 with [P4442][IDA] through multiple chemical sites. Figure adapted from "Chen et al. *Angewandte Chemie (International ed. in English)*, 55, 7166, 2016"[106]—Published by John Wiley and Sons.
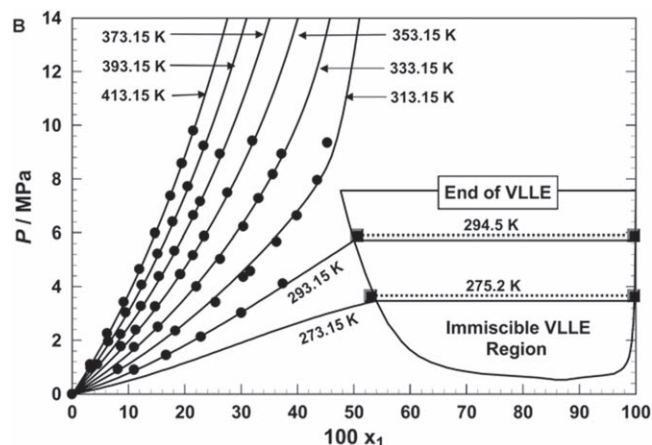
Figure 6. Phase equilibrium of [bmim][PF$_6$] and CO$_2$ at the temperature in the vicinity of CO$_2$ critical temperature. Lines represent the calculated data using Equation of State (EoS). The symbol x$_1$ represents the CO$_2$ molar fraction. Adapted with permission from (Shiflett et al. *Journal of Chemical & Engineering Data*, 55, 4785, 2010).[141] Copyright (2021) American Chemical Society.
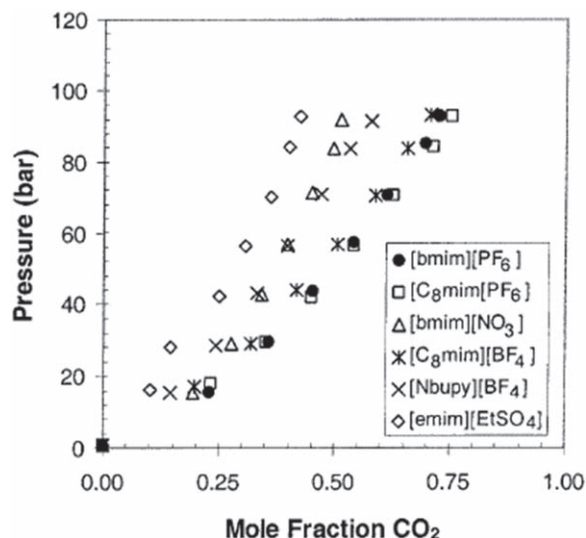
Figure 7. Phase equilibrium of typical CO$_2$-ILs mixtures for physical absorption of CO$_2$ at high pressure at 40 °C. Reprinted with permission from (Blanchard et al. *The Journal of Physical Chemistry B*, **105**, 2437, 2001).[8] Copyright (2021) American Chemical Society.

selectivity is also related to the careful control of empty space sizes, and CO$_2$ solubilization is related to inner empty space volume. It is also worth mentioning that selecting an IL for selectively absorbing CO$_2$ would also require knowledge about its interaction with the other gases. Previous studies reported that the ions' polarity plays a vital role in promoting selective CO$_2$/CH$_4$ absorption.[77]

High-pressure absorption.—The critical temperature (Tc) of CO$_2$ is 31.05 °C (or 304.2 K) which is a significantly low temperature.[130] In Fig. 6, it is possible to observe the phase equilibrium of [bmim][PF$_6$] and CO$_2$ in the vicinity of the CO$_2$ critical temperature. For isothermals below CO$_2$ critical temperature, IL + CO$_2$ mixture present liquid-liquid-vapor phase equilibrium. The gas-phase in thermodynamic equilibrium with a (liquid phase) IL- CO$_2$ binary mixture is supposedly composed of pure CO$_2$. There are many other reports[131–139] measuring phase behavior of CO$_2$ and IL mixture. According to Raeissi et al.,[139] a good design and optimization of application involving CO$_2$ and ILs requires accurate experimental data and also knowledge of the kind of phase behavior involved. The general classification of Scott and van Konynenburg[140] for binary mixtures at high pressures can be used to identify it. Knowing the CO$_2$ + IL phase behavior permits selecting the best experimental conditions and also using them as validation information for modeling and simulation purposes. Based on that, Raeissi et al.[139] discussed the most probable type of phase behavior for a mixture of CO$_2$ with imidazolium-based ILs.

The CO$_2$ physical absorption in ILs has been majority studied on the basis of experimental CO$_2$ solubility in ILs with varied pressure. Figure 7 shows a typical experimental finding pressure of binary mixtures is directly proportional to the CO$_2$ molar concentration.[6,137,142] The correspondence is very close to the ideal behavior described by Raoul's law. The current ATR-IR spectroscopic data provide strong evidence that the [BF$_4$]$^-$ anion interacting more strongly with CO$_2$ than [PF$_6$]$^-$, meaning that the strength of anion-CO$_2$ interaction decreases with the increase of anion size.[143] Thus, the strength of these anion-CO$_2$ interaction does is responsible for the solubility of CO$_2$ in imidazolium-based ionic liquids, but, very presumably, a free volume also play another important contribution. Blanchard et al.[8] noted a rough correlation between the liquid molar volume of the IL and CO$_2$ solubility. The IL molar volume, while not quantitative, gives an indication of "free volume" or "void space" available in the IL phase. Among the ILs investigated in Fig. 7, those ILs containing the largest molar volumes displayed also the highest CO$_2$ solubility. In fact, the linear correlation between CO$_2$ solubility and pressure (Fig. 7) suggests a space-filling mechanism.

Chemical CO$_2$ absorption in ILs.— *Brief theory.*—Since most TSILs use amine-based functional groups, these TSILs likely present
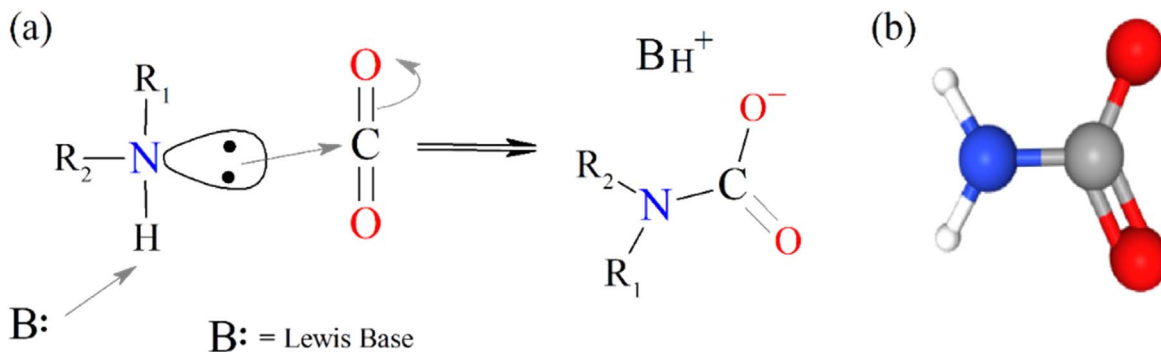
Figure 8. Sketch of the (a) CO$_2$ chemical interaction mechanism with primary and secondary amines, forming (b) carbamates. B: is a base acting as a proton acceptor/abstractor during the reaction and can be either water or even another alkanolamine. Adapted with permission from (Crooks &Donnellan, *Journal of the Chemical Society, Perkin Transactions 2*, 331, 1989)[147]—Published by The Royal Society of Chemistry.
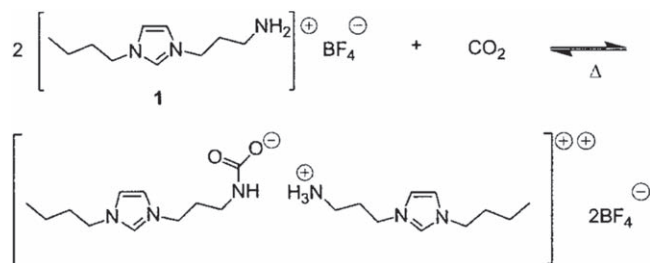
Figure 9. Proposed CO_2 reaction mechanism interaction with [Apbim][BF$_4$]. Reprinted with permission from (Bates et al. *Journal of the American Chemical Society*, **124**, 926, 2002).[92] Copyright (2021) American Chemical Society.

a chemical interaction with CO_2 as does aqueous amine. As initially proposed by Caplow (1968) and further developed by Danckwerts (1979), the reactional mechanism of CO_2 with either primary or secondary amines follows the scheme of Zwitterions,[92,144] which are compounds obtained upon the nucleophilic addition of N-hetero-cyclic carbenes (NHCs) onto carbon dioxide. The latest advances on the chemistry of the Zwitterions and related compounds can be consulted in the extensive Delaude's review.[145] In brief, the reaction begins with the donation of an electron pair from amine's nitrogen to the carbon of the CO_2 molecule,[146] forming a carbamate as shown in Fig. 8. The central amine is then deprotonated by a neighbor amine, or another Lewis base, stabilizing the carbamate by concentrating the negative charge over its C–O bond. For a primary and secondary amine, the global zwitterion-based reaction with CO_2 is shown below in reactions 6 and 7:

$$CO_2 + 2RNH_2 \rightleftharpoons RHNCOO^- + RNH_3^+, \quad [6]$$

$$CO_2 + 2RR'NH \rightleftharpoons RR'NCOO^- + RR'NH_2^+, \quad [7]$$

A similar reaction mechanism of carbamate formation upon CO_2 absorption into amines was proposed by Bates et al.[92] for an amine-functionalized IL, as shown in Fig. 9. The authors showed uncontestable experimental data based on infra-red and ^{13}C NMR spectroscopy confirming the characteristic absorption bands of carbamate for CO_2-rich 1-(3-propilamino)−3-butylimidazolium tetrafluoroborate, whose nomenclature is [Apbim][BF4]. ILs that chemically interact with CO_2 exhibited very promising CO_2-absorption capacities.[148,149] Among the growing number of chemical-absorber ILs, the [bmim][Ac] had attracted the most attention.[150–154] [bmim][Ac] has demonstrated to absorb CO_2 at high pressure by physical mechanism, displaying a substantial capacity of sorption induced by pressure. Amino-acid-functionalized ILs are highly viscous, which justifies the sluggish kinetics of CO_2 capturing. Despite this disadvantage, Brennecke, Schneider, and collaborators[101] verified 0.9 mol CO_2 per mol of [bmim][Ac] at room temperature and atmospheric pressure.

High-pressure absorption.—In terms of phase equilibrium, ILs that typically promote chemical interactions with CO_2 present a much higher absorption capacity and, therefore, lower vapor pressures. Thus, their IL-CO_2 phase equilibria behavior is no longer linear but exponential, as shown in Fig. 10.

High-Pressure CO_2 and CH_4 Solubilities In ILs

Experimental apparatus and measurements at high pressure.—The knowledge of the phase behavior of the CO_2 + IL systems at high pressure is very important for properly developing technologies using these compounds. The solubility of CO_2 in ILs has been determined experimentally by various researchers using different techniques. After an exhaustive search in the literature, we

concluded that the CO_2 + IL solubility data reported worldwide has been based mainly on four experimental techniques:

Isochoric method.—The isochoric method measures the gas absorbed by an IL in a closed system of a well-known volume, being such a closed system named Equilibrium Cell (EC). The EC equilibrium pressure is measured at the temperature settled by the thermostatic bath of the EC, cf. Fig. 11 and point 3. The mixture composition is changed by further addition of precisely-known amounts of CO_2 at a constant temperature, i.e the settled temperature by the bath at point 2 in Fig. 12. The way this amount of CO_2 is injected into the EC defines two main variants of the isochoric method. The solute injection may be either from a known volume of liquid CO_2[155] or from a gas reservoir whose volume can be precisely characterized whereas both the pressure and the temperature are monitored/controlled.[156] Thus, isotherms corresponding to CO_2 solubility at different pressure are obtained. This technique is also known as the **pressure drop method**. More details may be found elsewhere.[133–136] Note that the volume of the gas phase inside the EC is inferred as the difference between the total volume of EC and the volume of IL in the cell. For this reason, it is mandatory to consider the volume expansion of the IL due to the absorption of CO_2.

Differential weight.—This method is very simple. The ionic liquid is placed in an equilibrium cell with the gas. After equilibrium has been reached, a sample of the saturated-CO_2 ionic liquid is taken and weighted. Then, the sample is depressurized, vacuumed to remove all the dissolved gas, and weighted again. Differences between the two values are the mass of CO_2 dissolved in the liquid phase. This process is based on the assumption that the vapor pressure of ionic liquids is negligible. Details may be found elsewhere.[157] Figure 13 shows the experimental setup for this method.

Bubble point.—It is a widespread technique based on the vapor-liquid equilibrium, which is used for mixtures. The technique consists of producing a mixture with an exactly known composition. The mixture is subcooled in a variable volume view equilibrium cell. The volume is slowly increased (which reduces the pressure) at a constant temperature until the first bubble appears. Ionic liquids are considered to have a negligible vapor pressure. Therefore, the bubble pressure is approximately the saturation pressure of CO_2 in the CO_2 + IL mixture of well-known composition. The process may also occur at constant pressure, varying the temperature, i.e., either the pressure is gradually reduced whereas keeping the temperature constant (isothermal method) or the temperature is increased whereas keeping the pressure constant (isobaric method). When the first bubble is observed, the pressure (for the isothermal method) or the temperature (for the isobaric method) is recorded. The *PTx* variables indicate the saturation points, i.e., the solubility of CO_2 in the IL. Details may be found elsewhere.[157,159–162]

Gravimetric.—Gravimetric analysis is an analytical technique that describes the quantitative determination of the gas solubility by measuring the change in weight of a sample during absorption. A small portion of IL is placed on a high precision balance inside the equilibrium cell. The pressure of the system is raised by injecting CO_2. The mass change in the precision balance is a direct measurement of the gas dissolved in the IL. This technique directly measures the total mass of the solution at different CO_2 pressures. For this measurement, both the ionic liquid and the balance plate are immersed into the gas phase at different pressures. The weight measurements need to be corrected for buoyancy forces on the plate on the balance. The calculations are well described in the literature[163] and apparently, low uncertainties ($u_r(m_{CO_2})$ < 1%) have been achieved. A number of, many measurements can be
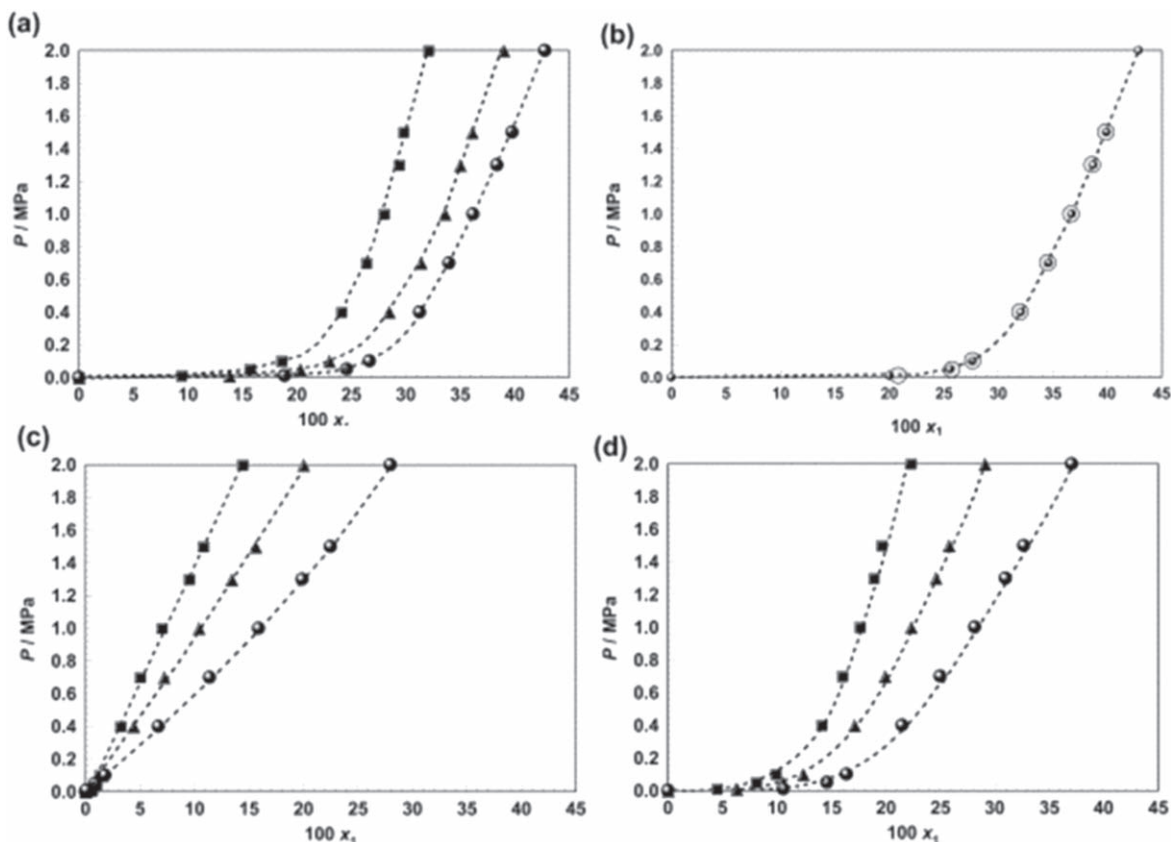
Figure 10. Phase equilibria of CO_2 + ILs known for promoting both physical and chemical interactions at ● 298.1 K; ○ desorption at 298.1 K; ▲ absorption at 323.1 K; and ■ absorption at 348.1 K (dashed lines, trend lines). Adapted with permission from (Shiflett & Yokozeki, *Journal of Chemical & Engineering Data*, **54**, 108, 2009).[142] Copyright (2021) American Chemical Society.
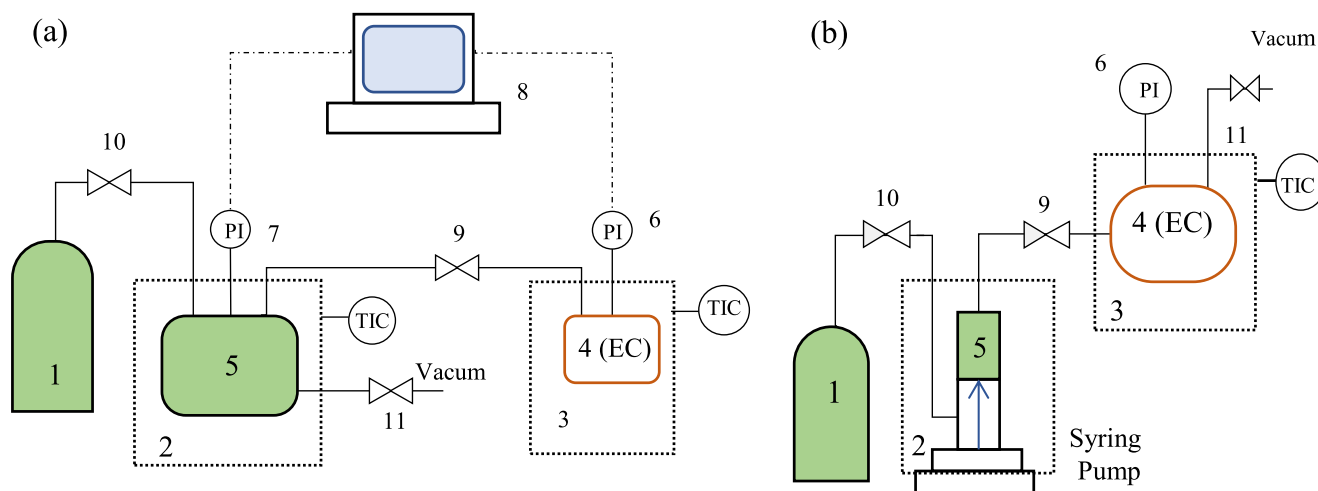
Figure 11. Schematic view of the isochoric system whereby the source of the solute is (a) in gaseous and (b) in liquid phases. 1- gas cylinder; 2 and 3- thermostatic baths; 4- equilibrium cell featuring precisely-known volume; 5- solute reservoir; 6 and 7- pressure transducers; 8- computer; 9- connecting valve; 10- inlet valve; 11- purge valve.

performed in short times. Details of this method may be found elsewhere.[137,138,157,164–167,158] Figure 13 shows a schematic view of a gravimetric system.

Influence of the liquid expansion in the solubility measurements.—The expansion of the liquid can have a significant effect on the measurement. For example, according to Jessop et al.,[168] at $P = 4$ MPa, ionic liquids can absorb about 10% of carbon dioxide which leads to a 10% increase in volume. For this expansion, the

measurement of the molality changes from $m = 2.5$ mol·kg^{-1}, when the expansion of the liquid is considered, to $m = 2.34$ mol·kg^{-1} when this expansion is neglected. This means a difference of 6.4% from the real value, which is higher than the uncertainty and it must therefore be taken into account.

Overview on the CO_2 selective solvents.—Several solvents could, at least in principle, enable the CO_2 separation via selective CO_2 absorption at high pressure. Different than those IL-based
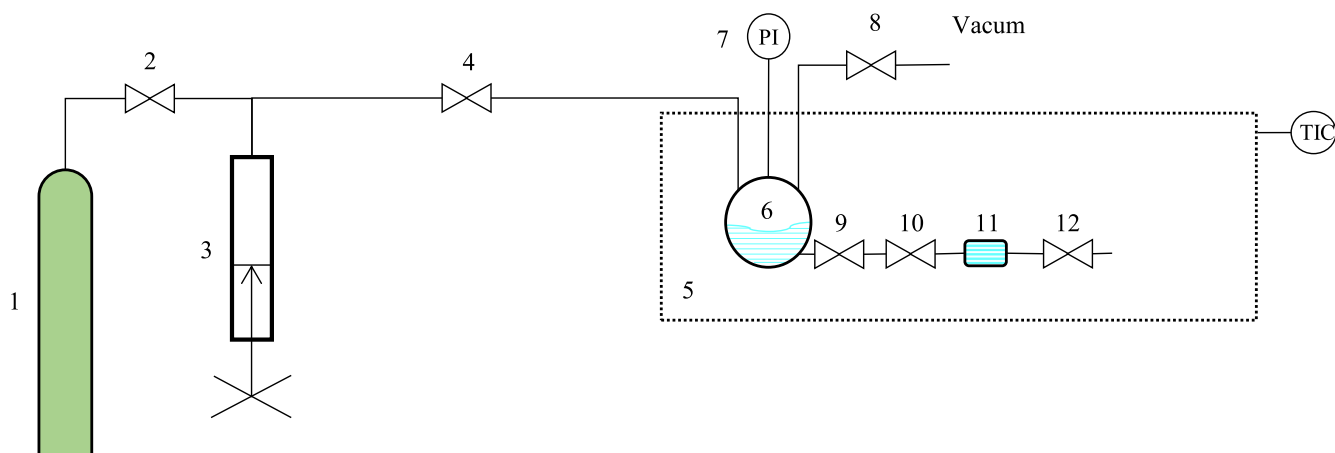
Figure 12. Differential weight experimental system. 1- CO_2 cylinder; 2- Hand screwing pump; 3- thermostatic air bath; 4- adjustable volume view equilibrium cell; 5- magnetic stirring plate; 6- liquid sampler.
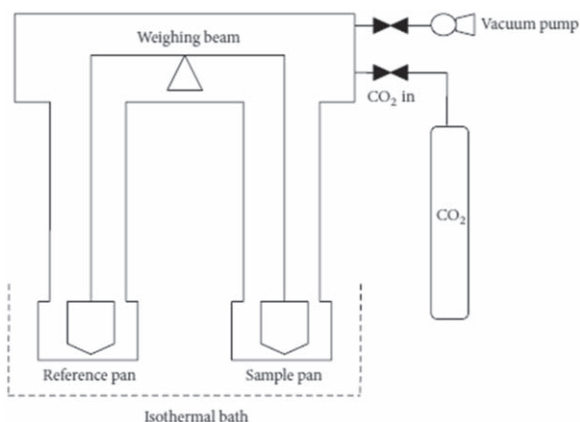
Figure 13. Schematic view of a gravimetric system reprinted with permission. Copyright © 2013 Elena Torralba-Calleja et al.[158]
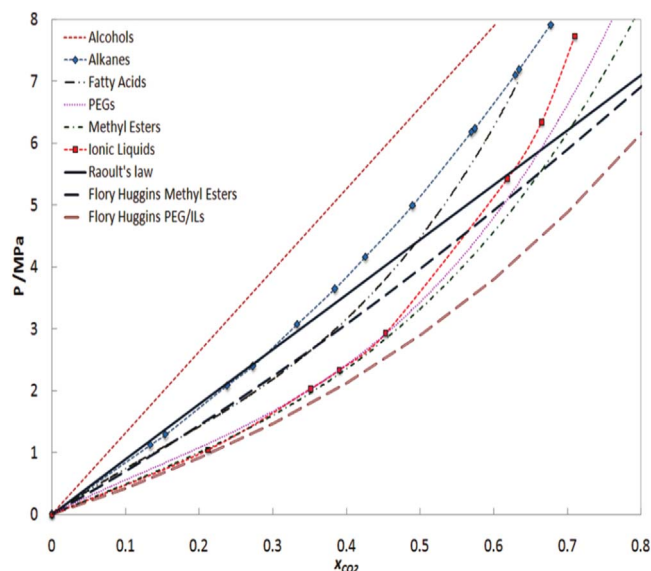
Figure 14. Sketch of binary CO_2 and solvents phase equilibrium at 313 K for six solvents, namely alcohol, alkenes, fatty acids, polyethylene glycol (PEG), methyl esters, and ionic liquids (IL). Adapted with permission from (P. J. Carvalho and J. A. P. Coutinho, *J. Phys. Chem. Lett.*, 1, 774, 2010).[9] Copyright (2021) American Chemical Society.

solvents described in section Design principles for ILs, to which the CO_2 absorptions occur mainly via a chemical interaction, other solvents like alcohols, alkenes, fatty acids, polyethylene glycols (PEGs), and methyl esters typically obey Raoult's law over some extend of CO_2 dissolution. This features a typical physical CO_2 absorption. Figure 14[9] shows the binary phase equilibrium with CO_2 for these solvents along with for an IL's representative. These solvents present in general a large molar volume, and the solute-solvent size and shape asymmetries generate significant entropic and free volume contributions, leading to deviation of an ideal solution (Raoult's law). Two other aspects have to be said about Fig. 14. These solvents feature vapor pressure inferior to 10^{-3} bar at room temperature, which is far above the 10^{-9} bar typically observed for ILs. As result, all those solvents would lose a considerable amount of material by evaporation during any industrial processes. Second, the IL vapor pressure line is much lower than other common physical absorbents, indicating that, in generic terms, ILs have higher CO_2 molar absorption capacity than other solvents.

Aqueous ethanolamines, developed in 1930, represent the most mature industrial adsorbent technology,[4] and since 1937 it has been applied to remove CO_2 from crude natural gas by the "Standard" oil company.[158] The most often employed amines for CO_2 capture are monoethanolamine (MEA), diethanolamine (DEA), methyldiethanolamine (MDEA), and more recently the diamines.[169,170] The reaction mechanism of CO_2 with amines involves the formation of carbamic acid and ion pair products.[146] The main disadvantages of aqueous amines are their high vapor pressure and volatility, corrosive potential, and the need for amine replacement after the regeneration cycle to compensate for the volatilized content at the beginning of the cycle.

Table II compares the CO_2 solubility capacities in aqueous amine against other chemical absorbents developed later on such as aqueous ammonium,[171,172] ionic liquids, and LI-based deep eutectic solvent (DES).[17,81–84,173–175] Even compared to reactive solvents, some ionic liquids, such as [P$_{4442}$][IDA], were observed to present significantly higher molar absorption capacity at low pressures.

Solubility of CO_2 and CH_4 in ILs at high pressure.—CO_2 solubilities at atmospheric pressure were extensively reported in section Design Principles for ILs. In Table III, the solubilities of both CO_2 and CH_4 are evaluated at supercritical pressures of CO_2, (scCO_2,) i.e. pressures above 50 bar. In practice, not the solubility but the selectivity is the key parameter for judging the separation performance. Hence, the solubility data in Table III assist to obtain the ideal selectivity, which is obtained by the solubility ratio of CO_2 to CH_4 at a constant temperature and pressure. Among the available experimental data, the highest selectivity of 11.16 (0.67/0.06) is found for [MMpy][eFAP] at ~50 bar and 40 °C,[177] followed by 6.88

Table II. Carbon dioxide solubilities in typical solvents.

CO_2 Solvents		Typical Solubility
1. Amine aq.		0.36 kg CO_2/kg MEA, Ref. 176
		0.5 mol CO_2/mol MEA
2. Ammonium aq.		0.9 kg CO_2/kg ammonium aq. @ $T = 70$ °C and $P = 63.5$ bar
(5 to 10 wt.%)		**0.368 mol CO_2/mol ammonium aq.**, Ref. 176
3. ILs	3.1 Pure ILs	**1.69 mol CO_2/mol** [P_{4442}][IDA] @ $T = 25$ °C and $P = 1.03$ bar, Ref. 106
		0.5 mol CO_2/mol [Apbim] [BF_4] @ $T = 25$ °C and $P = 1.03$ bar, Ref. 92
		0 mol de CO_2/mol [C4mim] [PF_6] @ $T = 40$ °C and $P = 1$ bar, Ref. 8
	3.2 DES	**0.399 mol CO_2/mol** ChCl/EG @ $T = 70$ °C and $P = 63.5$ bar, Ref. 17

(0.62/0.09) selectivity obtained with [C4mim][TFSI],[178] at similar conditions. A selectivity 4.18 (0.46/0.13)[a] is obtained for [C4mim] [Ac] at ~55 bar and 40 °C,[151] whereas a pressure-induced selectivity 4.23 (0.55/0.13) is obtained at ~270 bar and 30 °C.[179] Interestingly, ChCl/EG, that is a deep eutectic solvent of low viscosity and toxicity, exhibits a selectivity of 3.75 (0.060/0.016) at mild pressures (15 bar) and 40 °C.[89]

The gravimetric setup was employed for obtaining solubility data in Table III. Alternatively, if the bubble-point method is used to measure the vapor-liquid equilibrium, the ratio of Henry's law constant has to be estimated for obtaining the selectivities. A common approximation performed in the gas solubilities data obtained from the latter type of experiments is that the gas phase is only composed of the gas. Since the IL usually has vapor pressures below 10^{-5} bar,[24] it may be a feasible approximation for the bubble-point method. From such approximation, the gas solubilities can be easily estimated from the experimental data at low pressures or by a fitted thermodynamic model. Several equations of state (EoS) were previously used to fit the high-pressure data of gas-IL VLE, such as sPC-SAFT,[40] Soave-Redlich-Kwong,[181] and Peng-Robinson.[11] Most of which were used to calculate the fugacity coefficient in both phases with usually a simple cubic mixing rule, or they were only applied to represent the vapor-phase behavior. In the latter, the parameters of used Gibbs excess function, such as UNIQUAC and NRTL are adjusted to represent the high non-ideality behavior of ionic liquid systems.[182,183] In such cases, a suitable mixing rule must be applied, such as Wong-Sandler's or Huron-Vidal.

If any experimental data is not available, the adjusted models may be extrapolated to predict gas solubilities and selectivities at other conditions; however, without any great reliability of the estimated values. In such cases, predictive models may be more suitable approaches. Carvalho and Coutinho[9] reported an empirical method for the estimation of CO_2 solubility in ILs as a function of their molecular weights; however, only applied at a limited condition of low pressures. Predictive EoS can also be applied with properties predicted by Valderrama methods.[24,184,185] The predictive NRTL electrolyte,[186] LIFAC,[187] and COSMO-based methods can produce qualitatively suitable predictions.[182,188] From molecular simulation methods, the gas solubilities in ILs can be accurately predicted. These methods should account for low-distance interactions more precisely; therefore, also accounting for the important CO_2-anion interaction and the CO_2 accommodation into the IL inner voids.[148]

The models with regressed parameters may be interpolated to estimate the gas solubilities within the conditions evaluated by the experiments. For several years, Noble et al.,[189–192] proved the solubility of CO_2 and other light gases in imidazolium-based IL solvents can be modeled accurately using the regular solution theory (RST). Using a similar concept, high CO_2/CH_4 selectivity was reported for a few non-imidazolium-based IL ILs,[10,193] as displayed

in Fig. 15. The CO_2 dissolution in ILs proved to be an exothermic process,[111] and the decrease in CO_2 selectivity seen in Fig. 16 with the rising temperature corroborates with that.

To the best of our knowledge, only two papers have reported the CH_4 phase equilibrium behavior with ILs using the gravimetric setup and high pressures.[89,179] In general, the parameters of a thermodynamic model are regressed to represent the experimental data for N_2, which is well-known to display solubility in IL very similar to that of CH_4. Then, extrapolation or interpolation are performed to estimate the CH_4 solubility (or its N_2 equivalent) at the desired condition.[40,77,89,183,194] Both experimental and theoretical approaches display a linear-like CH_4 solubility at low gas composition, which is similar to that shown in Fig. 7. Previous studies reported the presence of a temperature crossover effect for some CH_4-IL VLE.[181] Furthermore, the CH_4 solubility in the IL may play an important role in their CO_2/CH_4 selectivity. Alcantara et al.[11] reported that ethanolamine-based ILs have much higher CO_2/CH_4 selectivity than several physical absorption imidazolium and pyridinium. Figure 16 displays the influence of the pressure on the CO_2 selectivity for a few ILs. For moderate pressures, that between 1 and 100 bar, the higher pressures reduce ILs selectivity. The compared ILs have similar CO_2 solubility; however, the much lower CH_4 solubility of ethanolamine-based ILs resulted in their higher selectivities reported.

Solubility and selectivity of H_2S and other gases.—Hydrogen sulfide is an acidic, corrosive, toxic, and flammable gas, that is widely found in the oil and gas industry. For these reasons, H_2S should be removed before further processing of either oil or natural gas. Typically, either the classic Claus process or a gas-liquid adsorption process using amine-based solvents are used.[195] However, the Claus process is only efficient for H_2S concentration above 55%, whereas the amine-based process suffers from poor H_2S selectivity. Fruitfully, this work addresses the ILs' employment to H_2S removal.

In the last two decades, the use of IL to adsorb H_2S was pointed out as a remarkably interesting solution to replace amines in the liquid-gas adsorption process.[141,196–202] In 2007, Jou & Mather[203] reported the adsorption of H_2S in ILs for the first time. The authors evaluated the solubility of H_2S in [bmim][PF6], concluding that the solubility of H_2S was strongly favored at higher pressures (90 bar) and at lower temperatures (25 °C). Later, Pomelli and co-workers produced one of the first reports that elucidated the mechanism of H_2S solubility in ILs using medium-pressure NMR spectroscopy. The authors observed that the solubility of H_2S was significantly higher than those reported for many other gases in ILs. In this case, the authors suggested that this higher solubility could be explained by the occurrence of specific interactions between H_2S since solubility decreases in the order $Cl^- > [BF_4^-] > [TfO^-] > [Tf_2N^-] > [PF_6^-]$. More recently, Hussein et al.[196] purposed a new molecular model based on an artificial neural network for predicting H_2S solubility in the presence of different ILs. For this, they collect data from the literature (1243 conditions), covering 33 different ILs. Their work provides an excellent tool to design novel ionic liquids for the H_2S separation process. Despite the success of these

[a]Carvalho et al.[89] found **0.46** mole fraction for CO2 dissolution in **[bmim][Ac]** at 55 bar, 40 °C, and 10^{-6} wt% humidity. Navarro et al. 152 found **0.11** mole fraction for CH4 dissolution in the same **[bmim][Ac]** at 200 bar, 30 °C, and zero wt% humidity. Despite the substantial mismatch in pressure between the measured solubilities, we calculate a **selectivity of 4.18** (0.46/0.11), even though this represents an underestimation (CO2 dissolution must increase from 55 to 200 bar, so the selectivity is well).

Table III. Solubility of both CO_2 and CH_4 in ILs using the gravimetric method at high pressures.

IL	CO_2 Solubility	CH_4 Solubility	Selectivity CO_2/CH_4	Humidity (mol IL: mol H_2O)	Pressure and Temperature	References
[thtdp][PF$_6$]	0.68	0.28	2.42	NA	50 bar, 40 °C	177
[MMpy][eFAP]	0.67	0.06	11.16	NA	50 bar, 40 °C	177
[bmim][TFSI]	0.62	0.09	6.88	NA	50 bar, 40 °C	178
[bmim][PF$_6$]	0.54	—	—	0.15 wt%	57 bar, 40 °C	8
[bmim][PF$_6$]	0.13	—	—	2.30 wt%	57 bar, 40 °C	8
[bmim][Ac]	—	0.07	—	33.33 mol% (2:1)	200 bar, 30 °C	179
[bmim][Ac]	—	0.11	—	0.00 mol% (1:0)	200 bar, 30 °C	179
[bmim][Ac]	0.46	—	4.18	10^{-6} wt%	55 bar, 40 °C	151
[bmim][Ac]	0.55	0.13	4.23	0.00 mol% (1:0)	270/280 bar, 30 °C	179
[bmim][Ac]	0.51	0.09	5.66	33.33 mol% (2:1)	240/280 bar, 40/30°C	179
ChCl/EG	0.06	0.016	3.75	NA	15 bar, 40 °C	89
[bmim][TFA]	0.51	—	—	10^{-6} wt%	55 bar, 40 °C	151
[emim][OTf]	0.65	—	—	0.00 wt%	100 bar, 40 °C	180
[emim][OTf]	0.58	—	—	10 wt%	100 bar, 40 °C	180
[emim][OTf]	0.51	—	—	10 wt%	60 bar, 40 °C	180
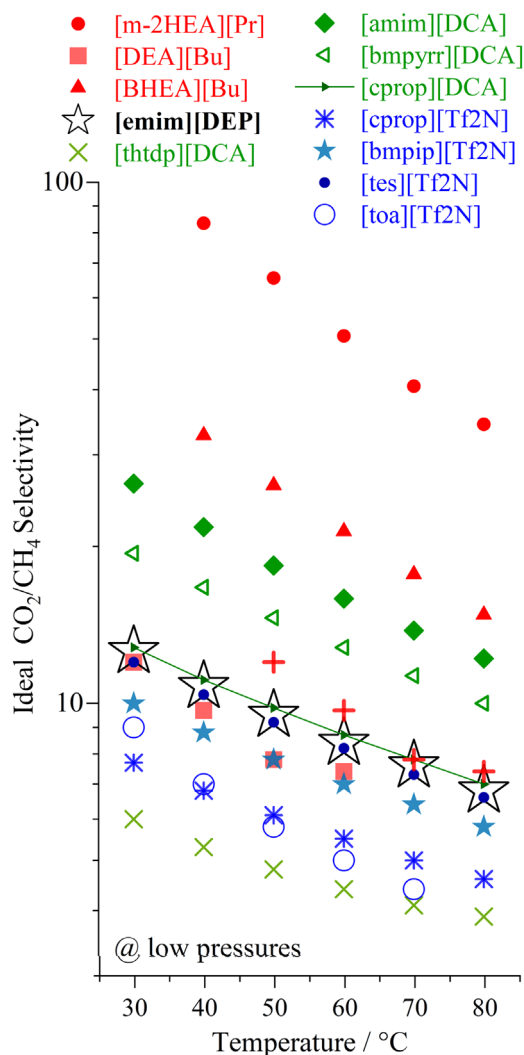
Figure 15. Ideal CO_2/CH_4 selectivity at low-pressure (between 1 and 60 bar) for [m-2HEA][Pr], [BHEA][Bu],[11] [DEA][Bu],[40] and others ILs.[159]

Figure 16. Ideal CO_2/CH_4 selectivity at 40 °C for [m-2HEA][Pr], [BHEA][Bu],[11] [DEA][Bu],[40] and others ILs.[159]

approaches, the application of this technology is still in its infancy mostly due to the prohibitive cost of this 2nd generation of ILs. Several authors have thus proposed different strategies, which go from using 3rd generation of ILs[204] to using IL-based membrane technologies[205–207] to perform the H_2S separation from different gaseous mixtures. For instance, Abdukarem et al.[204] have used molecular dynamic simulation to evaluate the transport of CO_2, H_2S, and CH_4 molecules across environmentally friendly choline-benzoate and choline-lactate ILs. The authors predicted exceptionally high CO_2/CH_4 and H_2S/CH_4 selectivities. Another insight was reported by Zhao et al.[205] that have synthesized different low-cost carboxylate protic ionic liquids to adsorb H_2S. Their results show that the length of the alkyl chains increases the solubility of H_2S in these ILs, which demonstrates that protic ILs could be a promising solution for H_2S separation.

The success obtained by ILs in the separation, in the adsorption of CO_2 and H_2S, or even in CH_4 has motivated several authors to evaluate their applicability in NH_3 adsorption.[208–213] For example, Makino e Kanakubo reported the solubilities and absorption mechanism in different types of IL. They verified that the Brønsted acidic ionic liquids, consisting of sulfo and carboxy groups and hydrogen sulfate anion, absorbed larger amounts of NH_3. Moreover, they also verified through Raman and NMR spectroscopy that NH_3 exhibits both physical and chemical adsorption. Another good example was brought by Kohler et al.[214] that have used

different SILPs to remove NH_3 irreversibly from an ambient gas (flow 1000 ppm NH_3 in N_2). The SILP was prepared by dispersion of thin films of imidazolium ILs onto a large surface area of polymer-based spherical activated carbon supports. Their results show that the increase in humidity significantly enhanced NH3 absorption in some of the studied SILPs.

Water influence on CO_2 solubility in IL.—Apparently, the effect of water on CO_2 solubilization in ionic liquids has been controversial.[129,215,216] The earliest experiments on the water effect on the IL CO_2 solubilization indicated a 75% reduction even at small water fractions. Blanchard et al.,[8] measured CO_2 molar fractions of 0.13 in high humidity against 0.54 in humidity-free [bmim][PF6] at 57 bar and 40°C. However, Table III presents a more precise scenario. Recent investigations indicate a much inferior impact of water on the CO_2 solubility in ILs.[179,180,215] Fu et al.[215] found a 15% reduction in CO_2 solubility for experiments reproducing the conditions originally used by Blanchard et al. and proposed some possible reasons for the mismatch: (a) instability of the anion [PF6], (b) presence of impurities, (c) IL degradation and so on. In another IL, [emim][OTf], CO_2 solubility was reduced by only 10% in presence of water.[180] Navarro et al.[179] observed that water fractions apply to better CO_2 selectivity in [bmim][Ac], even though both CO_2 and CH_4 solubilities reduce with water. Overall, CH_4 solubility is

reduced the most, in turn, favoring an enhanced CO_2 selectivity. For instance, Table III shows both CO_2 and CH_4 solubilities reduction in [bmim][Ac] from 0.55 to 0.51 and from 0.13 to 0.091, respectively, when in the presence of 33.33% of water at pressures between 280 a 240 bar, which results in an increase from 4.23 to 5.66 in CO_2 selectivity.

Such CO_2 absorption reduction with increasing water content in the IL was interpreted as a reduced Coulomb interaction among the ions in the presence of water[216]; or alternatively, it was interpreted as a competition of water and CO_2 for the same empty spaces.[129] However, at low water concentrations, the CO_2 solubility can be slightly higher than the water-free imidazolium ILs.[216] The ILs reaction with CO_2 may also benefit from the addition of small amounts of water.[217]

In a new interpretation, Bonilla et al.[218] proposed a reaction mechanism whereby, in addition to the reaction of the anion with CO_2 to form carbamate, the anion reacts with water (i.e., hydronium ions in water from either the natural dissociation of water or the formation of carbonic acid) and is reprotonated, leaving CO_2 to react with the hydroxide to form bicarbonate. This new route corroborates well with the recent interpretation from Jairton Dupont research group,[118,219] which advocates that the acid-base chemistry of buffer system plays an important role for superbase anions in the presence of water, recognizably known for its enhanced capacity of CO_2 absorption.

High-Pressure Processes for CO_2 Separation Employing ILs

The CO_2 removal from a stream of shale gas can increase its heat potential (for fuel streams), reduce equipment corrosion, and avoid its supersizing, resulting in economic gains and better safety. Several processes can be used for such separation,[220] such as absorption, membrane, adsorption, microbial conversion, and cryogenic distillation. For over eight decades, gas chemical absorption through aqueous alkanolamine remained the world-leading CO_2 capturing process due to its low cost, high absorption capacity, and selectivity.[221] However, these solvents are usually associated with equipment corrosion, high evaporation rates, and low thermal stability; which leads to foam formation and an efficiency reduction of the absorption processes.[222] Ionic liquids are emerging candidates to replace aqueous ethanolamine solutions mainly due to their low solvent loss and high CO_2 selectivity. Its negligible vapor pressure and higher thermal stability can promote lower solvent loss in absorption processes.[93,223] Besides, their overall high viscosity and tunable structures can promote lower solvent loss in supported ionic liquid membranes and facilitated transport mechanism membrane separation processes.[224,225]

IL-based absorption.—The CO_2 separation process employing ILs as absorbent occurs via selective absorption of CO_2 by chemical or physical interactions with the ILs. Briefly, Fig. 17 drafts an over-simplified separation process containing two steps, one unit for selective CO_2 capture and another for CO_2 stripping. In the absorption columns, a CO_2 rich gaseous stream flows upwards, while mixing with a counter-flow of a CO_2 selective IL stream. The stripping process, also known as desorption, consists of CO_2 removal from the CO_2–rich IL, which in turn regenerates the IL that is ready again to be used in the absorption unit, thus, closing the absorption/regeneration cycle (duty). Since CO_2 solubilization in the IL is exothermal, low temperatures and high pressures favor the CO_2 capture in the absorption unit. However, lowering the temperature may require utility consumption and might promote a significant viscosity increase, hampering the system's mass transfer and its overall efficiency. At the stripping unit, low pressures and high temperatures are preferable for promoting an easier absorbent recovery. However, too high temperatures may promote absorbent degradation,[222] and too low pressures are unfeasible at subsea conditions.

Presumably, the major bottleneck of IL-based absorbent for CO_2 separation processes at subsea pressure relates deeply with the

kinetics of the CO_2 adsorption/desorption process. The kinetics of CO_2 desorption is usually much more sluggish than its adsorption. Of course, the rate differences are deeply linked with the solvent and temperature used during the desorption process. In fact, the latter plays a major role in process economics. Usually, the desorption of CO_2 performed at temperatures above 100°C. This allows not only the recovery of CO_2 (e.g. Enhanced oil recovery - EOR) but also solvent regeneration which is an essential issue to the economic viability of the separation process.

In general, several others IL-non-related solvents suffer the same solvent-recyclability challenges. Although the slow kinetics of CO_2 adsorption was overcome through the use of numerous strategies namely the use of amines (e.g., monoethanolamine (MEA), piper-azine, and polyamines),[227] weak acids (e.g., boric acid),[228] amino acids (e.g., glycine and proline),[229,230] metal oxides (e.g., Al_2O_3, CuO, Fe_2O_3, SiO_2),[231,232] and carbon-based (e.g., graphene oxide) nanoparticles[233,234] or even enzymes (e.g., carbonic anhydrase),[235] the kinetics of desorption processes are still considered a major issue for most of the examples described above.

On the one hand, many efforts have been done to reduce the temperature of the IL-based CO_2 absorption step, as described in section Design principles for ILs. On the other hand, the use of phase change solvents has been one of the successful strategies to reduce the energy demand of the CO_2 desorption process. These solvents are aqueous or non-aqueous solutions amines, amino acids, or ionic liquids. The chemical interaction of CO_2 with these solutions promotes the formation of an immiscible phase richer in CO_2. This CO_2 richer phase can be separated and further processed to recover the CO_2 using a much lower energetic demand. The ILs also have proved to be suitable solutions to create these phase transfer solvents.[41,236–240] For example, Zhang et al.[238] reported a novel phase solvent based on a mixture of [TETA]Br-PMDETA with water which was able to absorb more than 2.6 mol of CO_2 per liter under 30 °C. Moreover, these solvents could be regenerated at 120 °C with a regeneration efficiency of 95% after four cycles.

Besides that, reversible ILs have also demonstrated the potential to address this subject. These ILs were firstly described by Jessop and co-workers.[239,240] These authors showed that certain ILs could be formed from nonionic liquids such as amine or alcohol when exposed to CO_2 leading to the formation of salt that could revert back to its initial state just by exposing it to an inert gas. This pioneering work has opened the doorways to different creative approaches for this type o ILs.[117,241,242] For instance, Huang and co-workers[243] described an interesting preorganization and coopera-tion strategy for highly efficient and reversible capture of low-concentration CO_2 by imide-based ILs. These authors show that this strategy allows considerable high adsorption of CO_2 (1.65 mol CO_2 per mol IL) and good reversibility (16 cycles).

In a recent hands-on processes review,[244] six promising imida-zolium and pyrrole-based ILs, known for promoting chemical interactions with CO_2, were evaluated in chemical absorption processes for CO_2 capture. The CO_2-IL reaction enthalpy and IL viscosity were identified as key properties to guide solvent selection. The IL performance in CO_2 capture processes was evaluated by means of solvent need, energy consume and column size. Among ILs studied, the [P$_{2228}$][CNPyr] resulted in the lowest column diameter required for the duty and the lower energy consumption. Its lower viscosity, high CO_2 solubility, and absorption kinetic resulted in a lower amount of ILs required for achieving the specifications; despite its high reacting energy of desorption. The reported results indicate that the studied ILs, especially the [P$_{2228}$][CNPyr], can be successfully used as CO_2 chemical absor-bents. The results also indicate that they can be competitive alternatives to current amine-based or aqueous ammonia technolo-gies for pre- and post-combustion CO_2 capture. However, at high pressure, [Bmim][Ac] may be more effectively applied for CO_2 capture due to its higher CO_2 solubility; possibly resulting in greater energy savings.
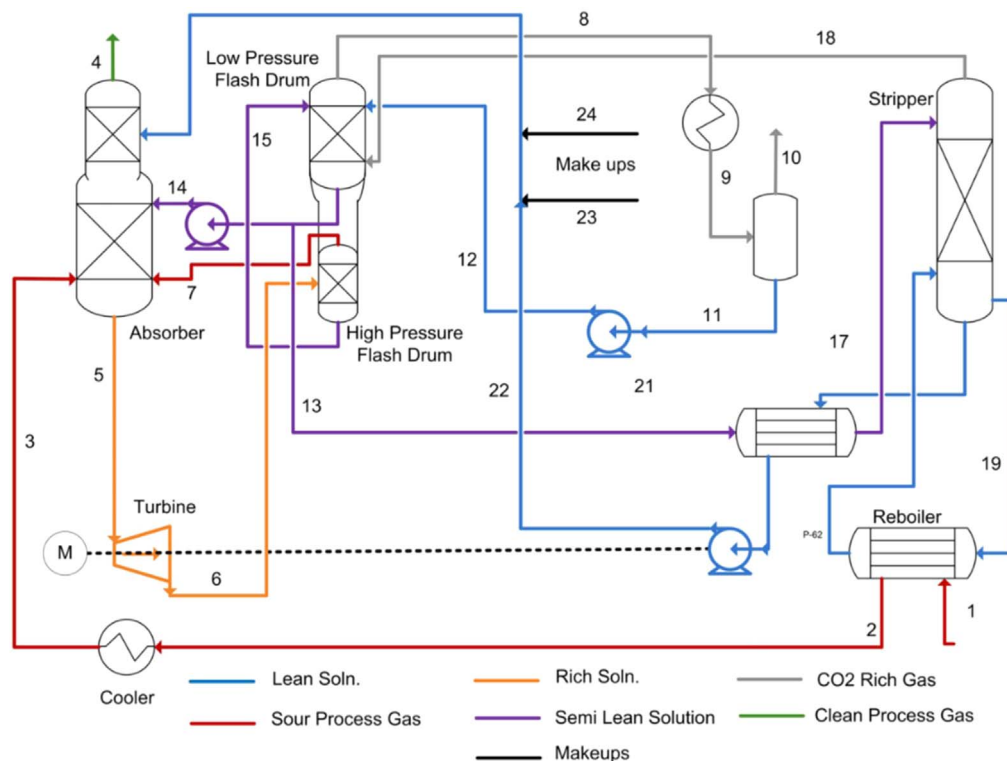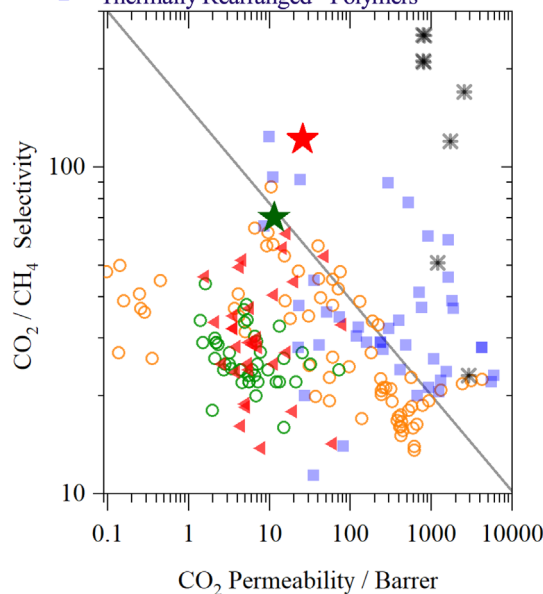
Figure 17. Sketch of a simple absorption unit for CO_2 separation. Reprinted from "Taimoor et al. *Processes*, 6 (2018)."[226]

IL-based membrane separation.—In short, the membrane gas separation process promotes a selective flow of a target specie through a physical barrier (membrane).[245] Despite recent advances,[217,246–248] the membrane-based technology is neither as mature nor cheaper than the current leading technology, i.e., alkanolamine-based absorption which has been optimized since 1931, right after Bottoms[4] deposited his patent. Recognizably, the main challenge for membrane-based separation is the suitable trade-off between membrane permeability and selectivity,[246] once highly permeable membranes lack selectivity and vice versa. The second, how to produce a membrane system with mechanical resistance and durability at high pressure.[217] If built with suitable materials and suitable micro- and nano-structures, the membrane-based separation would serve as efficient high-pressure gas separation. In general, organic-based materials have been the most frequently tested for IL-based CO_2 separation.[249] Alternatively, inorganic materials offer efficient ways to tailor pore sizes and shapes, known for regulating either permeability or selectivity. A few examples of inorganic materials are zeolites,[250,251] graphene and other two-dimensional 2D-atomically thin materials of the graphene family,[252] and carbon molecular sieve materials.[253] metal-organic frameworks (MOFs),[254]

Among the polymeric materials most used as membranes for CO_2/CH_4 separation are polyimide,[255–257] polysulfone,[258,259] thermally rearranged polymers,[76,260] and polycarbonates.[261,262] There are some strategies for combining ILs with polymeric membranes, which include: supported (or immobilized) ionic liquid membranes (SILMs), gel membranes, polymerized IL membranes (PILM), and IL composite membranes. To the best of our knowledge, membrane contactors have never tested for IL-based membranes, even though the reader finds an excellent up-to-data in the review by Nogalska et al.[263]

For convenient comparison in Fig. 18, the membrane separation performances are plotted on CO_2/CH_4 Robeson upper bound plots, being the different classes of materials color-coded. The graph collects data from the most recently updated reports.[247,264,265] Robeson's plots originally represent pure gas transport at dry and

Figure 18. Permeability/selectivity trade-off for polymeric membranes tuned either by the polymer chemical structure or by the IL-facilitated transport. Data collected from elsewhere.[247,264] SILM 1 refers to data from Alcantara et al.,[266] and SILM 2 refers to data from Alkhouzaam et al.[265]

ambient temperatures using purely polymeric homogeneous dense membranes. This plot compares the membranes' permeability and selectivity to the selected gases, being also conveniently used to compare the performance of different types of membranes, such as heterogeneous membranes or facilitated transport membranes that may require humidified gas streams. As seen in Fig. 18, many of the materials, especially thermally rearranged polymers and facilitated transport membranes surpass 2008 upper bound. Conventionally, the selectivity of purely polymeric homogeneous dense membranes such as polyimide and polysulfone substantially benefits from the insertion of ILs into its free volume space; however, polyvinyl alcohol (PVA) benefits the most, merely because of the higher intrinsic selectivity of the PVA matrix against the polysulfone, cf. SILM 1 against polysulfone and SILM 2 against polycarbonate and miscellanea.

Supported (or immobilized) ionic liquid membranes (SILM) are non-dispersive-type liquid membranes, in which ILs are immobilized inside the pores of porous support by capillary forces.[217,267–269] In principle, this concept may be used in both polymeric and inorganic porous supports; however, to the best of our knowledge, it has never been tested for a rigid inorganic supporter. The concept behind SILMs for polymeric membranes was firstly idealized and proved by Myers et al.[270] In principle, the transport of small gas molecules through polymers occurs by diffusion throughout transient free-volume elements or cavities formed by random, thermally stimulated motion of the flexible polymeric chains.[271] Myers et al. idealized that the specie formed by the chemical reaction of IL with CO_2 would serve as a transport carrier, once the CO_2 captured by the IL on the feed side of the membrane could diffuse throughout IL immobilized in the pores, and eventually, the reversible chemical reaction would free the CO_2 on the permeate side. The authors named this mechanism facilitated transport. We point out some a reservation on this topic. Originally, Myers et al. argued that the chemical reaction of CO_2 with IL was a complexation reaction, not an equilibrium system such as the coexistence of gaseous CO_2 with the aqueous solution rich in CO_3^{-2}. There is no guarantee that the reaction of CO_2 with ILs will be fully reversed at both the pressure and temperature swings allowed on the SILM permeate side on the seafloor. This issue can be addressed from different viewpoints. In this review, we decided to highlight those authors devoted to overcoming the energy penalty for the IL-regeneration, which the reader may find in section facilitated solvent regeneration.

Polymerized IL membranes (PILM) are those that incorporate ILs as monomers into the backbone chain forming the polymer molecule.[217] PILMs are known for their highly polar and ionic properties such as high conduciveness and high thermochemical resistance.[272] Some PILMs resulted in high CO_2 separation performance than its original IL.[273] Perhaps the major disadvantage of using PILMs in high-pressure CO_2 separation would be their overall low mechanical resistance.[217,274] An attempt to mitigate this problem includes the mixture of the PILMs matrix with polymers known for higher mechanical resistance. Recently, Dunn et al.[275] used a mixture of PILM with a suspension of zeolite in the same IL, which creates mixed matrix membrane (MMM), and reported CO_2/CH_4 separation characteristics under binary feeds up to 40 bar and 50 °C.

Another alternative is to use ILs is in gel membranes.[276] Among the common synthesizing routes, these membranes can be produced by adding a chelating agent to the selected IL followed by heat treatment. Due to their liquid-like properties, these membranes usually present high gas diffusion performances. However, these materials usually require thick membrane layers and may lose their original mechanical resistance at a high gas flow rate.

IL composite membranes are formed by the embedment of ILs into the polymeric material, forming a composite material that leads to an increase in both CO_2 permeability and selectivity.[217,277,278] The IL addition into a polymeric matrix modifies a set of polymeric membrane properties. This may promote a reduced diffusion of CO_2

and CH_4 gases; however, since the CH_4 diffusion is affected in a larger extension, the IL addition may result in a higher CO_2/CH_4 sorption selectivity.[277] Yet, it may increase the overall efficiency of the gas diffusion presumably due to an increase in polymer chain flexibility caused by a decrease in its crystallinity.[277,278] The latter effect may even be maximized by using a hygroscopic IL, as a consequence of the membrane swelling.[279] However, other properties are affected by ILs embedment, but negatively. The mixed IL matrix membranes are usually associated to lower thermal[277] and mechanical[279,280] resistances. The latter can be mitigated by blending the membranes with polymers featuring a higher mechanical resistance.[279]

facilitated solvent regeneration.—As stated in section Design principles for ILs, the ILs molecular structure can be tuned to promote higher CO_2 solubility by means of two major molecular strategies; whereas one strategy promotes the intimate chemical interaction between CO_2 and IL functional groups (including hydrogen bond), the other maximizes the free-volume of the ion structure for better accommodating CO_2 into it. However, the release of CO_2 from these two classes of absorbents is expected to exhibit substantially different CO_2-desorption kinetics at high pressure. In fact, there are just a few data on the CO_2 kinetics of desorption, yet all of them at 1 bar.[91,244,281] Considering the seafloor pressure of ca. 400 bar and minimum suitable subsea pressure of 200 bar, the kinetic of CO_2 desorption is expected to be highly disfavored in the subsea condition. For this reason, our viewpoint on the (electro-) catalysis-induced separation process is now considered. The main reason for treating this topic aside grounds on subsea high pressure to be, now, an asset, and not a mitigated problem as discussed in section named IL-based absorption. Both the kinetic rate of electro-catalysis and homogeneous catalysis will benefit from the $scCO_2$ pressure as large as 400 bar.

Hereby, the reader finds our thoughts on very risky but promising endeavors to facilitate CO_2 desorption/separation, being three of them briefly mentioned below. Actually, they represent a new way of "thinking" about the separation processes, in which CO_2 is absorbed via chemical reaction, thus forming a second phase that can be either methanol[282] or formic acid,[283] i.e. CO_2 separation by a chemical-reaction induced phase-transition.

Catalyst-aided IL-regeneration.—Heterogeneous mesoporous catalysts rich in Bronsted-acid sites have been tested by Bairq et al.[284] as solid sorbents to enhance the CO_2 desorption rate. The authors enhanced the desorption rate by 195%, and a decreased energy requirement by 37.41% compared to the monoethanolamine as a blank run. Despite proved for the mature amine solvent, we believe this concept can potentially be suitable for IL as well. A recent review on this topic offers more details.[285]

Regeneration aided by homogenous CO_2 electro-reduction.—Imidazolium-based salts are known to act as a molecular co-catalyst for homogenous CO_2 reduction. Taking advantage of this fact, Weilhard et al.[286] employed ILs in the selective hydrogenation of CO_2 to formic acid (FA) and proved it to be efficient. Furthermore, the authors proposed that FA would be separated upon the immobilization of IL followed by simple filtration.

Regeneration aided by electrocatalysis.—In this concept, the solid electrified electrode is employed in IL-regeneration without entering in direct contact with the CO_2, but exclusively with the IL-cation, which is reduced at the solid electrified catalyst. This concept is inspired by the homogeneous electroreduction of CO_2 by organic promoters.[282,283,287] For instance, Lim et al.[283] report chemical, homogeneous CO_2 reduction to the formate anion ($HCOO-$) by a metal-free benzimidazole-based organo-hydride. In principle, the absorbed CO_2 is readily reduced by the benzimidazole-based hydride donor, which is then oxidized to its aromatic
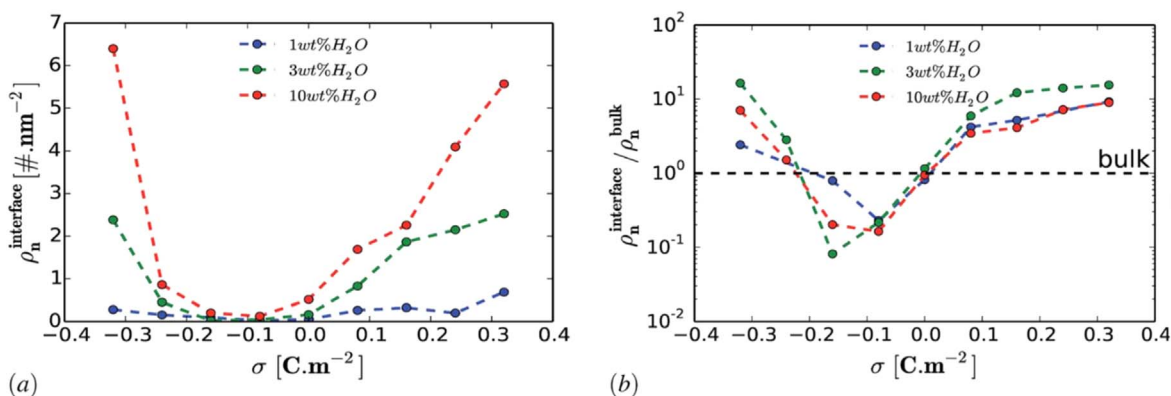
Figure 19. Electrosorption of water on graphene from water-containing reline (chcl: urea 1:2) contacting a graphene interface. The averaged (a) and normalized (b) number density of adsorbed water in the interfacial region as a function of surface charge density. The number of residual water molecules in bulk Reline is 1 wt%, 3 wt%, and 10 wt%. The interfacial region is taken to be 3.5 Å from the graphene surface. Reproduced from "Mamme et al. *Nanoscale Advances*, **1**, 2847, 2019"[288]—Published by The Royal Society of Chemistry.

benzimidazolium cation. Then such cation is electrochemically reduced to its original organo-hydride form on the solid electrode, establishing its recyclability.

CO$_2$ (Electro)Catalysis Either in IL or at High-Pressures

Both the high pressure and the use of IL as electrolytes can benefit the CO$_2$RR. The use of IL replacing water as electrolyte greatly promises to impact the properties on the electrified solid/liquid interface. ILs electrochemical window is wider than that of water, which enables a far larger number of other reduction reactions to take place with substantial kinetic performance since the water reduction can no longer hide them. In the context of the CO$_2$ electro–reduction (CO$_2$RR), enlarged chances of either favoring this target reduction or promoting the carbon-carbon coupling are envisioned.

In a recent review, Dong et al.[13] put together a few theoretical and experimental understandings on the EDL for the IL/metal interface, being the latest, additional advances briefly highlighted hereby. Mamme et al.[288] evaluate the amount of adsorbed water in the vicinity of the interface between reline (chcl: urea 1:2) and a negatively charged graphene electrode, i.e. electric field similar to CO$_2$RR polarity. Figure 19 shows the main results. Regardless of the water concentrations in IL, the adsorbed water tends to increase in the interfacial region with a charged electrode, cf. plate (a). For the moderately negatively charged graphene electrode, the water molecules are depleted compared to the bulk, cf. plate (b). Besides, a further increase in surface charge density of the negatively charged electrode ($\sigma < -0.16$ C·m^{-2}) leads to an increase in water adsorption. This is mainly due to the enhancement of the electrostatic interaction between the charged graphene electrode and the water molecules. For highly charged electrodes, water adsorbs at both electrodes due to a strongly enhanced external electrostatic interaction between the electrodes and the water dipoles. This allows more free spaces for the accumulation of more water molecules in the vicinity of the negatively charged surface, which features a more compact conformation when compared to the positively charged electrode.

Figure 20 shows in detail the alignments of water and IL-cation on the electrode. On the uncharged electrode, Fig. 20b, there is no preferential orientation of any of the molecules; instead, both are oriented randomly. However, when the electrode is charged negatively/positively both polar molecules show a preferential orientation. At the negatively charged electrode (blue electrode), Fig. 20a, both IL-cation and water molecules are aligned in a mixture of perpendicular and parallel arrangements, i.e., the H–O–H plane of water is perpendicular and parallel to the graphene electrode, respectively.

Major issues of ILs for electrocatalysis.—The IL viscosity is by far the major challenge for using ILs in electrocatalysis. Despite the
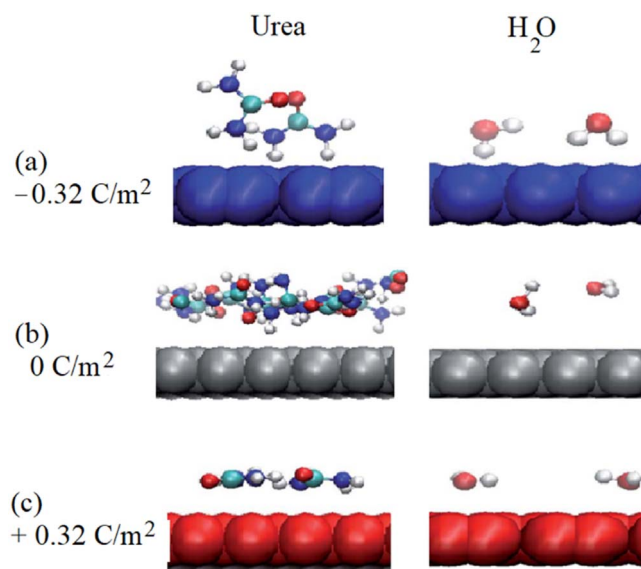
Figure 20. Orientation of IL-cation (Urea) and water molecules near the electrode surface for different surface polarizations -0.32 C·m^{-2} (a), 0 C·m^{-2} (b) and $+0.32$ C·m^{-2} (c). The total water content was 3 wt%. The uncharged electrode is colored grey, whereas negatively and positively charged electrodes are colored blue and red, respectively. The color-coding of the atoms of IL-cation and water is: white, hydrogen; cyan, carbon; blue, nitrogen; and red, oxygen. Reproduced from 'Mamme et al. *Nanoscale Advances*, **1**, 2847, 2019'[288]—Published by The Royal Society of Chemistry.

elevated ionic degree, the ionic conductivities of some ILs are greatly lowered with the high viscosity owing to the low mobility of the charge carriers, cf. Stokes-Einstein relationship in Eq. 1, vide section Properties. Further, other mass-transport-related issues feature the electrocatalysis in ILs such as the products/reactant mass transport and bubble entrapment. For example, Fig. 21 depicts some dramatic images of bubble entrapment during a rotating disk electrode experiment carried out with [DEA][HSO4], which is the most viscous IL listed in Fig. 3. A selection of electrolytes for CO$_2$-based electrosynthesis has to be based on a conjunct analysis of both viscosity and ionic conductivity, to which the Walden plot offers valuable guidelines for IL selection.

Zhao et al.[39] highlights a bunch of other viscosity-related issues like (a) the necessity of adding an unusually large content of supporting electrolyte (inorganic salts like NaSO$_4$) in order to achieve measurable Faradic currents; (b) enlarged chances of the electrochemical cell to operate under the ohm domain, instead of the
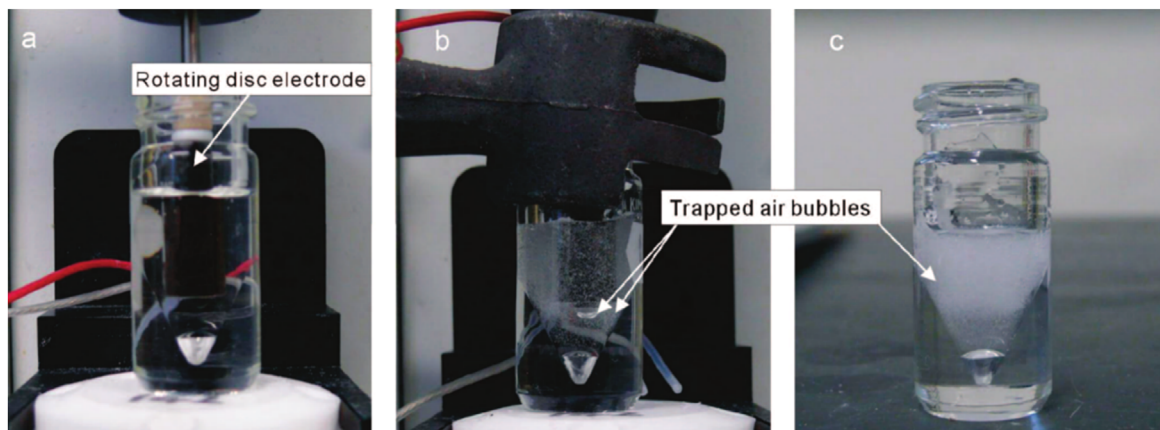
Figure 21. Photographs of an electrochemical cell (a) before, (b) during, and (c) after a rotating disk voltammetric experiment in the viscous ionic liquid, [DEA] [HSO4]. Image b was taken after rotation for 30 s at 1000 rpm, and image c was taken 30 min after the experiment. Reprinted with permission from (Zhao et al. *The Journal of Physical Chemistry B*, **112**, 6923, 2008).[39] Copyright (2021) American Chemical Society.

Faradaic domain; (c) the bubble entrapment mitigate against the achievement of a Levich limiting current under RDE conditions; and (d) highly viscous media also may result in the adsorption of colbaltocene or ferrocene or their precipitation at the IL/interface, which restricts their use for reference potential scale purposes.

Further complications arrive from the development of a reference scale for the electrical potential. Knowing the formal potential by means of an electrochemical probe, named as reference electrode (RE), is central to understand the underlying processes at the IL/ metal interface. The electrical potential drop at the RE electrode has to be related to the free energy of Gibbs, which is mathematically expressed in terms of the Nernst equation. So that, the electro-chemical probe has (a) to obey the Nernst equation, (b) to be fully reversible over both positive and negative sides of the potential scale, (c) to provide a fast equilibrium restore under the action of any small potential perturbation, and (d) to be stable over time. If, otherwise, the electrochemical probe fulfills all the requirements except the item (a), as does the silver (Ag) wire in contact with the IL, the electrode is said pseudo-reference, and the potential despite measurable has no physical meaning in absolute terms, being suitable only to study variations on the potential, i.e. the potential window. In aqueous media, both the widely known hydrogen evolution (HER/$2H^+ \rightarrow H_2$) and hydrogen oxidation (HOR/$H_2 \rightarrow 2H^+$) reactions fulfill that set of requirements, leading to the widespread use of H_2/H^+ pair as RE in aqueous media; but, unfortunately, it proved unsuitable on IL media. According to Meng et al.,[289] the cyclic Voltammograms of the H_2/H^+ redox couple in imidazolium-based IL exhibits a quasi-reversible feature on the HER side of the potential scale, which in addition were also substantially dependent on the nature of IL anion. Until 2008 and 2010, the major advances in the development of RE for ILs can be found reviewed by Zhao et al.[39] and Barrosse-Antle et al.,[290] respectively. In more recent years, Compton & Students[289,291–297] have intensified the search of different redox pairs suitable at the IL/ metal interface, which led the researchers to study some of the fundamental processes at this interface by the very earliest time, and it has been of great assistance to standardize the way in which electrochemical experiments in ILs are approached.

In non-aqueous electrolytes, such as organic solvents, the International Union of Pure and Applied Chemistry (IUPAC) recommends the use of the redox ferrocene/ferrocenium, $[Fe(C_5H_5)_2]/[Fe(C_5H_5)_2]^+$, couple as an inner reference scale, being the recommended abbreviation Fc/Fc$^+$.[298,299] A reference probe is pragmatically prepared by dissolving equimolar amounts of ferrocene and ferrocenium hexafluorophosphate [Fc][PF$_6$] to give between 4 mM to 30 mM solution in IL, which in addition may contain an extra salt as a supporting electrolyte if dealing with an IL of poor ionic conduction.[300] However, issues like Fc poor solubility[301] and

volatility of dissolved ferrocene under vacuum conditions[302,303] demonstrated to restrict its use as RE for potential calibration. Further, RE manufacturing has to follow a stringent protocol to avoid contamination by dissolved gases such as oxygen and others in the atmosphere, so that the headspace of the RE compartment has to be subject to evacuation by vacuum before electrochemical measurements. According to Compton & students,[303] this protocol ensures that even if the Fc is volatilized by the low-pressure environment, accurate RE data can be still obtained. The researchers have even modified the Fc structure to mitigate its volatilization under vacuum.[292] Unlike most cells for the study of aqueous electrolytes, the IL-based RE employed a specific cell featuring an IL drop deposited on the electrode disk.[304] Alternatively, Bond and co-workers[301] have demonstrated that the Cobaltocenium/ Cobaltocene redox couple ($[Co(C_5H_5)_2]^+/[Co(C_5H_5)_2]$) hereafter referred to as Cc$^+$/Cc) probably is a broadly superior reference scale in both organic solvent and in ILs on the bases of both the Cc$^+$ negligible volatility and generally high solubility of Cc+. In aprotic ILs, [Cc][PF$_6$] (36.5–450.0 mM) was found to be much more soluble than Fc (27.5–101.8 mM), whereas the diffusion coefficient D, estimated by the classical Stokes-Einstein equation, for Fc^0 and Cc$^+$ does not change significantly with concentration.[294] This supports the use of both Fc^0 and Cc$^+$ to provide a well-characterized and model redox couple for use as a voltammetric internal potential reference.

In practical terms, however, the use of a silver (Ag), gold (Au), or platinum (Pt) wire as a pseudo-reference electrode, in which wires are immersed directly into the IL, had been widespread because of its simplicity and the fact that possible contamination of test IL is avoided. To date, senior surface electrochemists adopt the Ag pseudo-RE without further referencing to either Fc^0 or Cc$^+$ in the IL tested. It may be argued that Ag pseudo-RE presents a stable potential, so that its formal potential against either Fc or Cc + using Ag wire can be accurately gauged any time later, either after each experiment or after the data publication. In experimental practice, preparation of IL-based RE on daily basis is humanely unfeasible, whereas using Fc or Cc + based RE prepared any time before the day of experimental record adds substantial uncertainty on the formal potential. The accurate measure of the formal potentials is central to understand surface electrochemistry, and comparison of the measurements allows redox data to be reported against either Fc or Cc + in an aqueous solution. The formal potential of H$^+$/H$_2$ redox couple on Pt in [C2mim][Tf2N] was quantified as –0.065 V at 25 °C vs Fc/Fc$^+$ (or –0.338 V vs Ag/Ag+).[305] For larger, coordinatively saturated specie such as Fc and Cc$^+$, the IL-based variations in formal potential tend to be small,[306] so that it is judged unnecessary to list formal potentials in more than one IL; however, the same can not be extended to the redox couple containing smaller ions such as

H $^+$/H$_2$ and Ag+/Ag redox couple that must be measured for each IL. Furthermore, the difference between formal electrode potentials of Fc/Fc$^+$ and Cc$^+$/Cc redox couples was 1.34 V, enabling conversion between the two internal potential Refs. [307], [308].

CO$_2$RR in neat and dissolved ILs.—All the experimental assessments of the CO$_2$RR in ILs reported the production of single-carbon molecules (C1), which substantially differs from aqueous-based electrocatalysis that is capable to synthesize two-carbon molecules (C2) as the major product. In the recent review of Chen & Mu[309] the reader may found compiled a broad number of varied experimental conditions used to promote CO$_2$RR in IL worldwide, all of them leading to the C1 and carbon monoxide as major products. Unfortunately, ILs-mediated CO$_2$ electro-reduction into higher-carbon-chain products as the major products were not reported yet.

The south Brazilian research group of Jairton Dupont has been reported comprehensive advances on the CO$_2$RR in neat ILs. For instance, Faggion et al.[310] critically discussed the electrochemical reduction of CO$_2$ considering selected recent examples. The authors highlighted that ILs play a significant role due to their distinct physical chemistry properties, the tuning of the reactions conditions, the assistance with radical CO·− in overpotential, and the increase in faradaic efficiency and current density. Alternatively, the ILs are dissolved in an organic solvent. For instance, Wellington et al.[311] employed aqueous electrolytes containing the ionic liquid (IL) 1-n-butyl-2,3-dimethylimidazolium acetate ([BMMIm][OAc]) and di-methyl sulfoxide (DMSO) as the electrolyte, and reported that CO$_2$RR proceeds at low overpotentials (−0.9 V vs Ag/AgCl) at commercially-available Au electrodes, and with high selectivity for

CO production (58% faradaic efficiency at −1.6 V vs Ag/AgCl). Furthermore, the authors discuss the possible reaction pathways involved in the CO$_2$ reduction to CO in IL buffer-like solutions. They had observed 0.43 mol of CO$_2$ per mol of IL dissolved into the electrolyte at atmospheric pressure, forming bicarbonate and providing a constant supply of dissolved CO$_2$ to the electrode. This equilibrium with bicarbonate can be shifted with confined water activation by the IL anion structure, which acts like a neutral base catalyst as well as a proton buffer.

Using the IL-dissolved approach, Feaster et al.[312] determined that [EMIM][Cl] breaks down at both the working and counter electrodes under reaction conditions under both acidic and basic conditions. The authors used 1 H nuclear magnetic resonance spectroscopy on the electrolyte before and after electrolysis. Such electro-activity of the ILs-cations at the electrode underscores the challenges in employing ionic liquids for CO$_2$RR. Still using IL-dissolved approach, Sun at. al.[313] noted a shift on the reaction course by promoting the formation of carbon monoxide instead of oxalate anion. We have one reservation on the IL-dissolved approach. It is highly probable that EDL has a remarkably distinct structure and properties when considered the electrode in contact with neat and diluted ILs. It is not certain whether both cases exhibit similar distributions of adsorbates.

Electrocatalysis at high pressure.—Hori[314] argues that the increasing CO$_2$ partial pressure up to 60 bar has a minor impact on the adsorption energy of CO on the electrode surface, which is the initially adsorbed intermediate along the CO$_2$RR. In this context, the apparent benefit of the CO$_2$RR with an increased pressure derives from a higher CO$_2$ concentration in the electrolyte solution at high pressure, cf. Fig. [14]. Interestingly, the LIs are the most suitable electrolyte to absorb CO$_2$ at high pressures, outperforming any other in terms of phase stability whereas retaining more than a half CO$_2$ molar ratio. At this point, we discuss the possibility of synthesizing hydrocarbons from a CO$_2$-enriched IL at high pressure.

Thanks to the pressures around 100 bar, the syngas (H$_2$ mixed with CO) were converted into light hydrocarbons (those having up to eleven carbon centers) by the first time over alkalized iron chips, which is known as the Fischer-Tropsch (FT) synthesis.[315] Contrariwise, heavy hydrocarbons can be produced at lower pressure (∼7 bar). To date, the total syngas pressure is widely known to influence both the FT kinetics and the FT catalyst surface structure. The pressure of 20–30 bar generally results in condensation of hydrocarbons flooding the catalyst pores by liquefied products, which, in turn, slows down the mass transfer of reagents. The shortening hydrocarbon chain with high pressure has been be interpreted in the context of reagent concentrations and reagent mass transfer in the gaseous and liquid phases. Further, total pressure can influence the catalytic surface restructuring at the atomic level, which affects the number of active sites in cobalt catalysts. Scanning transmission microscopy has shown significant restructuring of the cobalt Co (0001) surface in the presence of H$_2$/CO = 2 mixture at 4 bar and 250 °C. Industrial FT units typically employ cobalt catalysts and operate at 220 °C–240 °C, a total pressure of 20–30 bar, and an inlet H$_2$/CO ratio of 1.7 to 2.2. The reader is referred to Khodakov et al.[315] for global review and to Weststrate et al.[316,317] for a current understanding of the structure sensitivity and on the surface chemistry of growing chains.

There is no electro-catalytic version of the FT processes. Figure [22] get into perspective the most efficient electrochemical platforms for CO$_2$RR in terms of faradaic efficiency (FE).[318–325] At atmospheric pressure, conventional electrocatalysis enables efficient CO$_2$ reduction to two-carbon-containing molecules such as ethylene (60% FE), ethanol (85% FE), and oxalate (76% FE). Those molecules couple two carbons centers and indicate that the carbon-carbon bound can be promoted by electrified surfaces. Comparatively, the electrified plasma-liquid interface (PLI) enables the highest CO$_2$RR efficiency ever, about 98% efficiency; however, it is only suitable at atmospheric pressure. At high pressure,
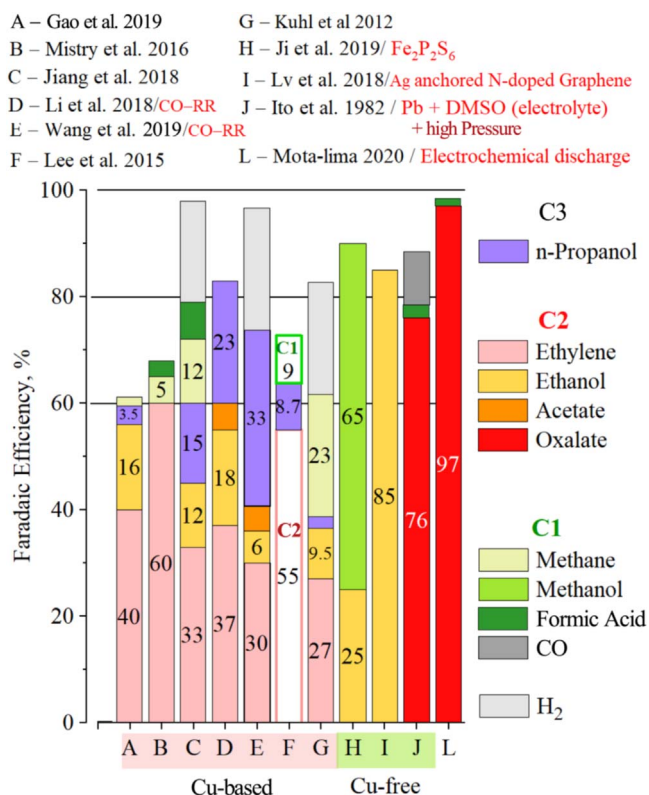
Figure 22. Faradaic efficiency of CO$_2$ electroreduction on copper-based electrocatalysts (references A−G), copper-free electrocatalysts (references H−J), or a catalyst-free platform (L) based on a range spectrum of the final products (C3, n-propanol; C2, ethylene, ethanol, acetate, and oxalate; C1, methane, methanol, formic acid, and carbon monoxide; and hydrogen). References D and E tested the carbon monoxide reduction reaction. Reprinted with permission from (A. Mota-Lima, *J. Phys. Chem. C*, **124**, 10907, 2020).[327] Copyright (2021) American Chemical Society.

electrosynthesis of oxalic acid (to which oxalate is the conjugate base) needs ∼9.6 bar to reach 76.6 % FE in the non-aqueous electrolyte when performing CO_2RR on the lead electrode.[326] How would the lead electrode perform CO_2RR at 200 bar in ILs?

Aside from the catalyst selection based on the desired final product, the design of the high-pressure reactor is an additional, but not secondary, challenge. The already well-established electrolyzers for pressure smoothly above the atmospheric level unsuits the mechanical constrictions imposed by the supercritical CO_2 (⩾50 bar). At sea level, the reactor has to have a thicker wall to support the difference between inner and outer pressure without blowing the reactor up. In this context, further innovation on the Membrane Electrode Assembly (MEA) was already published by Ramdin et al.,[328] and the new MEA allowed the facile flow of any catholyte (CO_2-enriched IL, for example) at the anode compartment at high pressure. Despite being a semicontinuous batch reactor, such a high-pressure electrolyzer successfully converts CO_2 to formic acid. At the subsea level, we foresee that such innovations may be employed; however, without the capital expenditure for a thicker wall reactor, once the inner and outer pressure should no longer be so dissimilar at subsea.

Conclusions

Recovering natural gas at extremely high pressure on the seafloor is a current challenge to exploit undersea natural gas resources. This review critically evaluates possible ways to employ Ionic Liquid (IL) for CO_2 separation from natural gas on the seafloor, meaning the total pressures can vary between 400 and 200 bar. The main drawbacks to implement either an IL-based membrane or a recyclable IL-absorbent for the selective capture of CO_2 are thoroughly analyzed. With enthusiasm, we discuss the value of CO_2 electro-reduction either for assisting IL-regeneration or for paving new ways for further CO_2 processing in the context of the carbon-neutral industry. In either case, CO_2 selectivity, IL viscosity, and intrinsic ionic conduction of the ILs are key properties to be considered to select the best candidate for an application, the reason for which this review carefully evaluates them, compiling the most updated data.

ORCID

Andressa Mota-Lima https://orcid.org/0000-0002-6820-9797
Murilo Leite Alcantara https://orcid.org/0000-0002-4312-1836
Fernando J. Pérez-Sanz https://orcid.org/0000-0003-3911-7284
Reinaldo C. Bazito https://orcid.org/0000-0002-8768-8308
Pedro Vidinha https://orcid.org/0000-0002-3907-4969
Rita M. B. Alves https://orcid.org/0000-0002-1914-5133
Claudio A. Oller Nascimento https://orcid.org/0000-0001-6110-0249

References

1. A. C. N. Amaral, P. M. d. Carvalho, J. M. F. Coelho, and A. P. d. A. Mendes et al., *Estudo sobre o aproveitamento do Gás Natural do Pré-sal*, Ministerio de Minas e Energia, Natural-Gas-Department, Brazil Governement (2020), Brasília, Brazil, http://www.anp.gov.br/arquivos/estudos/ingles-aproveitamento-gn-pre-sal.pdf.
2. K. Dalane, Z. Dai, G. Mogseth, M. Hillestad, and L. Deng, *J. Nat. Gas Sci. Eng.*, **39**, 101 (2017).
3. F. A. Albuquerque, F. L. V. Vianna, R. P. Alves, C. Kuchpil, M. G. G. Morais, R. T. C. Orlowski, C. A. C. Moraes, and O. Ribeiro, *Offshore Technology Conference*, Houston, Texas, USA (2013), https://onepetro.org/OTCONF/proceedings-abstract/13OTC/All-13OTC/OTC-24161-MS/37686.
4. R. R. Bottoms, *Industrial & Engineering Chemistry*, **23**, 501 (1931).
5. P. V. Danckwerts, *Chem. Eng. Sci.*, **34**, 443 (1979).
6. L. A. Blanchard, D. Hancu, E. J. Beckman, and J. F. Brennecke, *Nature*, **399**, 28 (1999).
7. Y. Wang, X. Liu, A. Kraslawski, J. Gao, and P. Cui, *J. Clean. Prod.*, **213**, 480 (2019).
8. L. A. Blanchard, Z. Gu, and J. F. Brennecke, *J. Phys. Chem. B*, **105**, 2437 (2001).
9. P. J. Carvalho and J. A. P. Coutinho, *J. Phys. Chem. Lett.*, **1**, 774 (2010).
10. M. Hasib-ur-Rahman, M. Siaj, and F. Larachi, *Chem. Eng. Process.*, **49**, 313 (2010).
11. M. L. Alcantara, P. I. S. Ferreira, G. O. Pisoni, A. K. Silva, L. Cardozo-Filho, L. M. Lião, C. A. M. Pires, and S. Mattedi, *Sep. Purif. Technol.*, **196**, 32 (2018).
12. Z. Lei, C. Dai, and B. Chen, *Chem. Rev.*, **114**, 1289 (2014).
13. K. Dong, X. Liu, H. Dong, X. Zhang, and S. Zhang, *Chem. Rev.*, **117**, 6636 (2017).
14. S. Zeng, X. Zhang, L. Bai, X. Zhang, H. Wang, J. Wang, D. Bao, M. Li, X. Liu, and S. Zhang, *Chem. Rev.*, **117**, 9625 (2017).
15. T. L. Greaves and C. J. Drummond, *Chem. Rev.*, **115**, 11379 (2015).
16. Y. Huang, Y. Zhang, and H. Xing, *Chin. J. Chem. Eng.*, **27**, 1374 (2019).
17. Y. Zhang, X. Ji, and X. Lu, *Renew. Sustain. Energy Rev.*, **97**, 436 (2018).
18. V. M. Blasucci, R. Hart, P. Pollet, C. L. Liotta, and C. A. Eckert, *Fluid Phase Equilib.*, **294**, 1 (2010).
19. K. N. Marsh, J. A. Boxall, and R. Lichtenthaler, *Fluid Phase Equilib.*, **219**, 93 (2004).
20. B. Monteiro, L. Maria, A. Cruz, J. M. Carretas, J. Marçalo, and J. P. Leal, *Thermochim. Acta*, **684**, 178482 (2020).
21. M. J. Earle, J. M. S. S. Esperança, M. A. Gilea, J. N. Canongia Lopes, L. P. N. Rebelo, J. W. Magee, K. R. Seddon, and J. A. Widegren, *Nature*, **439**, 831 (2006).
22. M. H. Joshipura, *Indian Chem. Eng.*, **57**, 154 (2015).
23. J. Hekayati, A. Roosta, and J. Javanmardi, *J. Mol. Liq.*, **225**, 118 (2017).
24. J. O. Valderrama and L. A. Forero, *Fluid Phase Equilib.*, **317**, 77 (2012).
25. F. Ferrarini, G. B. Flôres, A. R. Muniz, and R. P. de Soares, *AIChE J.*, **64**, 3443 (2018).
26. T. L. Greaves and C. J. Drummond, *Chem. Rev.*, **108**, 206 (2008).
27. S. Aparicio, M. Atilhan, and F. Karadas, *Ind. Eng. Chem. Res.*, **49**, 9580 (2010).
28. C. Maton, N. D. Vos, and C. V. Stevens, *Chem. Soc. Rev.*, **42**, 5963 (2013).
29. M. V. S. Oliveira, B. T. Vidal, C. M. Melo, R. D. C. M. de Miranda, C. M. F. Soares, J. A. P. Coutinho, S. P. M. Ventura, S. Mattedi, and Á. S. Lima, *Chemosphere*, **147**, 460 (2016).
30. N. M. C. Talavera-Prieto, A. G. M. Ferreira, P. N. Simões, P. J. Carvalho, S. Mattedi, and J. A. P. Coutinho, *The J. Chem. Thermodyn.*, **68**, 221 (2014).
31. J. A. Widegren and J. W. Magee, *Journal of Chemical & Engineering Data*, **52**, 2331 (2007).
32. M. C. Corvo, J. Sardinha, S. C. Menezes, S. Einloft, M. Seferin, J. Dupont, T. Casimiro, and E. J. Cabrita, *Angew. Chem. Int. Ed.*, **52**, 13024 (2013).
33. C. Cadena, J. L. Anthony, J. K. Shah, T. I. Morrow, J. F. Brennecke, and E. J. Maginn, *JACS*, **126**, 5300 (2004).
34. M. G. Freire, A. R. R. Teles, M. A. A. Rocha, B. Schröder, C. M. S. S. Neves, P. J. Carvalho, D. V. Evtuguin, L. M. N. B. F. Santos, and J. A. P. Coutinho, *Journal of Chemical & Engineering Data*, **56**, 4813 (2011).
35. Y. Xu, *The Journal of Chemical Thermodynamics*, **64**, 126 (2013).
36. B. K. Chennuri and R. L. Gardas, *Fluid Phase Equilib.*, **427**, 282 (2016).
37. U. Domańska and M. Królikowska, *J. Solution Chem.*, **41**, 1422 (2012).
38. M. Iglesias, R. Gonzalez-Olmos, I. Cota, and F. Medina, *Chem. Eng. J.*, **162**, 802 (2010).
39. C. Zhao, G. Burrell, A. A. J. Torriero, F. Separovic, N. F. Dunlop, D. R. MacFarlane, and A. M. Bond, *The J. Phys. Chem. B*, **112**, 6923 (2008).
40. M. L. Alcantara, J. P. Santos, M. Loreno, P. I. S. Ferreira, M. L. L. Paredes, L. Cardozo-Filho, A. K. Silva, L. M. Lião, C. A. M. Pires, and S. Mattedi, *Fluid Phase Equilib.*, **459**, 30 (2018).
41. T. L. Greaves, A. Weerawardena, C. Fong, I. Krodkiewska, and C. J. Drummond, *J. Phys. Chem. B*, **110**, 22479 (2006).
42. D. P. Rimmer, A. A. Gregoli, J. A. Hamshar, and E. Yildirim, *Emulsions* (American Chemical Society, Washington, DC) p. 295 (1992).
43. L. Hakim, Y. Ishii, K. Matsumoto, R. Hagiwara, K. Ohara, Y. Umebayashi, and N. Matubayasi, *J. Phys. Chem. B*, **124**, 7291 (2020).
44. P. Walden, *Z. Phys. Chem.*, **55**U, 207 (1906).
45. W. Yoshizawa, W. Xu, and C. A. Angell, *JACS*, **125**, 15411 (2003).
46. A. Noda, K. Hayamizu, and M. Watanabe, *J. Phys. Chem. B*, **105**, 4603 (2001).
47. T.-Y. Wu, S.-G. Su, Y.-C. Lin, H. P. Wang, M.-W. Lin, S.-T. Gung, and I. W. Sun, *Electrochim. Acta*, **56**, 853 (2010).
48. A. I. Bhatt and G. A. Snook, *Handbook of Reference Electrodes*, ed. G. Inzelt, A. Lewenstam, and F. Scholz (Springer, Berlin, Heidelberg) 7, p. 189 (2013).
49. W. Xu and C. A. Angell, *Science*, **302**, 422 (2003).
50. M. S. Miran, H. Kinoshita, T. Yasuda, M. A. B. H. Susan, and M. Watanabe, *Phys. Chem. Chem. Phys.*, **14**, 5178 (2012).
51. M. S. Miran, H. Kinoshita, T. Yasuda, M. A. B. H. Susan, and M. Watanabe, *Chem. Commun.*, **47**, 12676 (2011).
52. M. S. Miran, T. Yasuda, M. A. B. H. Susan, K. Dokko, and M. Watanabe, *RSC Adv.*, **3**, 4141 (2013).
53. M. S. Miran, T. Yasuda, R. Tatara, M. A. B. H. Susan, and M. Watanabe, *Faraday Discuss.*, **206**, 353 (2018).
54. W. Xu, E. I. Cooper, and C. A. Angell, *J. Phys. Chem. B*, **107**, 6170 (2003).
55. D. R. MacFarlane, M. Forsyth, E. I. Izgorodina, A. P. Abbott, G. Annat, and K. Fraser, *Phys. Chem. Chem. Phys.*, **11**, 4962 (2009).
56. P. Kumar Sahu, A. Ghosh, and M. Sarkar, *J. Phys. Chem. B*, **119**, 14221 (2015).
57. D. Rauber, F. Philippi, J. Zapp, G. Kickelbick, H. Natter, and R. Hempelmann, *RSC Adv.*, **8**, 41639 (2018).

58. G. L. Burrell, I. M. Burgar, Q. Gong, N. F. Dunlop, and F. Separovic, *J. Phys. Chem. B*, **114**, 11436 (2010).
59. M. Kunze, M. Montanino, G. B. Appetecchi, S. Jeong, M. Schönhoff, M. Winter, and S. Passerini, *The Journal of Physical Chemistry A*, **114**, 1776 (2010).
60. C. I. Daniel, F. Vaca Chávez, G. Feio, C. A. M. Portugal, J. G. Crespo, and P. J. Sebastião, *J. Phys. Chem. B*, **117**, 11877 (2013).
61. C. Iacob, J. R. Sangoro, P. Papadopoulos, T. Schubert, S. Naumov, R. Valiullin, J. Kärger, and F. Kremer, *Phys. Chem. Chem. Phys.*, **12**, 13798 (2010).
62. J. R. Sangoro, C. Iacob, S. Naumov, R. Valiullin, H. Rexhausen, J. Hunger, R. Buchner, V. Strehmel, J. Kärger, and F. Kremer, *Soft Matter*, **7**, 1678 (2011).
63. H. Tokuda, S. Tsuzuki, M. A. B. H. Susan, K. Hayamizu, and M. Watanabe, *J. Phys. Chem. B*, **110**, 19593 (2006).
64. O. Nordness and J. F. Brennecke, *Chem. Rev.*, **120**, 12873 (2020).
65. Z. Wojnarowska, Y. Wang, K. J. Paluch, A. P. Sokolov, and M. Paluch, *Phys. Chem. Chem. Phys.*, **16**, 9123 (2014).
66. S. K. Mann, S. P. Brown, and D. R. MacFarlane, *Chem. Phys. Chem*, **21**, 1444 (2020).
67. A. Serbanovic, Ž. Petrovski, M. Manic, C. S. Marques, G. V. S. M. Carrera, L. C. Branco, C. A. M. Afonso, and M. Nunes da Ponte, *Fluid Phase Equilib.*, **294**, 121 (2010).
68. J. Pitawala, A. Matic, A. Martinelli, P. Jacobsson, V. Koch, and F. Croce, *J. Phys. Chem. B*, **113**, 10607 (2009).
69. A. I. M. C. Lobo Ferreira, A. S. M. C. Rodrigues, M. Villas, E. Tojo, L. P. N. Rebelo, and L. M. N. B. F. Santos, *ACS Sustainable Chem. & Eng.*, **7**, 2989 (2019).
70. S. Balchandani, B. Mandal, and S. Dharaskar, *Fluid Phase Equilib.*, 112643 (2020).
71. J. Yang, X. Yu, J. Yan, and S.-T. Tu, *Ind. Eng. Chem. Res.*, **53**, 2790 (2014).
72. U. Kapoor and J. K. Shah, *J. Phys. Chem. B*, **122**, 9763 (2018).
73. L. F. Lepre, L. Pison, L. J. A. Siqueira, R. A. Ando, and M. F. Costa Gomes, *Sep. Purif. Technol.*, **196**, 10 (2018).
74. S. Aparicio, M. Atilhan, M. Khraisheh, and R. Alcalde, *J. Phys. Chem. B*, **115**, 12473 (2011).
75. K. A. Kurnia, F. Harris, C. D. Wilfred, M. I. A. Mutalib, and T. Murugesan, *The Journal of Chemical Thermodynamics*, **41**, 1069 (2009).
76. Y. F. Yeong, H. Wang, K. P. Pramoda, and T.-S. Chung, *J. Membr. Sci.*, **397–398**, 51 (2012).
77. P. J. Carvalho and J. A. P. Coutinho, *Energy Environ. Sci.*, **4**, 4614 (2011).
78. T. Welton, *Chem. Rev.*, **99**, 2071 (1999).
79. S. Mattedi, P. J. Carvalho, J. A. P. Coutinho, V. H. Alvarez, and M. Iglesias, *The Journal of Supercritical Fluids*, **56**, 224 (2011).
80. J. L. McDonald, R. E. Sykora, P. Hixon, A. Mirjafari, and J. H. Davis, *Environ. Chem. Lett.*, **12**, 201 (2014).
81. A. P. Abbott, G. Capper, D. L. Davies, H. L. Munro, R. K. Rasheed, and V. Tambyrajah, *Chem. Commun.*, 2010 (2001).
82. A. P. Abbott, G. Capper, D. L. Davies, R. K. Rasheed, and V. Tambyrajah, *Chem. Commun.*, **70**, 224 (2003).
83. A. P. Abbott, D. Boothby, G. Capper, D. L. Davies, and R. K. Rasheed, *JACS*, **126**, 9142 (2004).
84. B. Gurkan, H. Squire, and E. Pentzer, *J. Phys. Chem. Lett.*, **10**, 7956 (2019).
85. L. L. Sze, S. Pandey, S. Ravula, S. Pandey, H. Zhao, G. A. Baker, and S. N. Baker, *ACS Sustainable Chem. & Eng.*, **2**, 2117 (2014).
86. N. Zhang, Z. Huang, H. Zhang, J. Ma, B. Jiang, and L. Zhang, *Ind. Eng. Chem. Res.*, **58**, 13321 (2019).
87. X. Wang, D. Shang, S. Zeng, Y. Wang, X. Zhang, X. Zhang, and J. Liu, *The Journal of Chemical Thermodynamics*, **128**, 415 (2019).
88. T. J. Trivedi, J. H. Lee, H. J. Lee, Y. K. Jeong, and J. W. Choi, *Green Chem.*, **18**, 2834 (2016).
89. M. B. Haider, D. Jha, B. M. Sivagnanam, and R. Kumar, *J. Environ. Chem. Eng.*, **7**, 102747 (2019).
90. M. B. Haider, D. Jha, B. M. Sivagnanam, and R. Kumar, *Journal of Chemical & Engineering Data*, **63**, 2671 (2018).
91. H. Yan, L. Zhao, Y. Bai, F. Li, H. Dong, H. Wang, X. Zhang, and S. Zeng, *ACS Sustainable Chem. & Eng.*, **8**, 2523 (2020).
92. E. D. Bates, R. D. Mayton, I. Ntai, and J. H. Davis, *JACS*, **124**, 926 (2002).
93. J. Zhang, C. Jia, H. Dong, J. Wang, X. Zhang, and S. Zhang, *Ind. Eng. Chem. Res.*, **52**, 5835 (2013).
94. M. Pan, R. Vijayaraghavan, F. Zhou, M. Kar, H. Li, C. Wang, and D. R. MacFarlane, *Chem. Commun.*, **53**, 5950 (2017).
95. J. Wu, B. Lv, X. Wu, Z. Zhou, and G. Jing, *ACS Sustainable Chem. & Eng.*, **7**, 7312 (2019).
96. M. Pan, Y. Zhao, X. Zeng, and J. Zou, *Energy & Fuels*, **32**, 6130 (2018).
97. Q. Yang, Z. Wang, Z. Bao, Z. Zhang, Y. Yang, Q. Ren, H. Xing, and S. Dai, *Chem. Sus. Chem*, **9**, 806 (2016).
98. Z. Zhang, L. Zhang, L. He, W.-L. Yuan, D. Xu, and G.-H. Tao, *The J. Phys. Chem. B*, **123**, 6536 (2019).
99. B. F. Goodrich, J. C. de la Fuente, B. E. Gurkan, Z. K. Lopez, E. A. Price, Y. Huang, and J. F. Brennecke, *J. Phys. Chem. B*, **115**, 9140 (2011).
100. Y. Zhang, S. Zhang, X. Lu, Q. Zhou, W. Fan, and X. Zhang, *Chemistry—A European Journal*, **15**, 3003 (2009).
101. B. E. Gurkan, J. C. de la Fuente, E. M. Mindrup, L. E. Ficke, B. F. Goodrich, E. A. Price, W. F. Schneider, and J. F. Brennecke, *JACS*, **132**, 2116 (2010).
102. B. E. Gurkan, T. R. Gohndrone, M. J. McCready, and J. F. Brennecke, *Phys. Chem. Chem. Phys.: PCCP*, **15**, 7796 (2013).
103. I. Niedermaier et al., *JACS*, **136**, 436 (2014).
104. J. L. Anthony, J. L. Anderson, E. J. Maginn, and J. F. Brennecke, *J. Phys. Chem. B*, **109**, 6366 (2005).
105. O. Hollóczki, Z. Kelemen, L. Könczöl, D. Szieberth, L. Nyulászi, A. Stark, and B. Kirchner, *ChemPhysChem*, **14**, 315 (2013).
106. F. F. Chen, K. Huang, Y. Zhou, Z. Q. Tian, X. Zhu, D. J. Tao, D. E. Jiang, and S. Dai, *Angewandte Chemie (International ed. in English)*, **55**, 7166 (2016).
107. J. E. Bara, C. J. Gabriel, S. Lessmann, T. K. Carlisle, A. Finotello, D. L. Gin, and R. D. Noble, *Ind. Eng. Chem. Res.*, **46**, 5380 (2007).
108. Z.-B. Zhou, H. Matsumoto, and K. Tatsumi, *Chemistry—A European Journal*, **11**, 752 (2005).
109. K. Tsunashima and M. Sugiya, *Electrochem. Commun.*, **9**, 2353 (2007).
110. Y. Deng, S. Morrissey, N. Gathergood, A. M. Delort, P. Husson, and M. F. C. Gomes, *Chem. Sus. Chem*, **3**, 377 (2010).
111. L. Zhou, X. Shang, J. Fan, and J. Wang, *The Journal of Chemical Thermodynamics*, **103**, 292 (2016).
112. M. Kanakubo, T. Makino, T. Taniguchi, T. Nokami, and T. Itoh, *ACS Sustainable Chem. & Eng.*, **4**, 525 (2016).
113. S. Tang, G. A. Baker, and H. Zhao, *Chem. Soc. Rev.*, **41**, 4030 (2012).
114. C. Wang, H. Luo, D.-E. Jiang, H. Li, and S. Dai, *Angew. Chem. Int.*, **49**, 5978 (2010).
115. R. Li, Y. Zhao, Z. Li, Y. Wu, J. Wang, and Z. Liu, *Science China Chemistry*, **62**, 256 (2019).
116. C. Wang, X. Luo, H. Luo, D.-E. Jiang, H. Li, and S. Dai, *Angew. Chem. Int.*, **50**, 4918 (2011).
117. F. Li, Y. Bai, S. Zeng, X. Liang, H. Wang, F. Huo, and X. Zhang, *Int. J. Greenhouse Gas Control*, **90**, 102801 (2019).
118. M. Zanatta, N. M. Simon, and J. Dupont, *Chem. Sus. Chem*, **13**, 3101 (2020).
119. A. S. Shalygin, N. S. Nesterov, S. A. Prikhod'ko, N. Y. Adonin, O. N. Martyanov, and S. G. Kazarian, *J. Mol. Liq.*, **315**, 113694 (2020).
120. T. Seki, J.-D. Grunwaldt, and A. Baiker, *J. Phys. Chem. B*, **113**, 114 (2009).
121. L. M. dos Santos, F. L. Bernard, B. B. Polesso, I. S. Pinto, C. C. Frankenberg, M. C. Corvo, P. L. Almeida, E. Cabrita, and S. Einloft, *J. Environ. Manage.*, **268**, 110340 (2020).
122. M. Zanatta, M. Lopes, E. J. Cabrita, C. E. S. Bernardes, and M. C. Corvo, *Journal of CO₂ Utilization*, **41**, 101225 (2020).
123. S. Moret, P. J. Dyson, and G. Laurenczy, *Dalton Trans.*, **42**, 4353 (2013).
124. S. M. Silva, R. P. J. Bronger, Z. Freixa, J. Dupont, and P. W. N. M. van Leeuwen, *New J. Chem.*, **27**, 1294 (2003).
125. J. K. Moore, J. A. Surface, A. Brenner, P. Skemer, M. S. Conradi, and S. E. Hayes, *Environmental Science & Technology*, **49**, 657 (2015).
126. G. Laurenczy, S. Jedner, E. Alessio, and P. J. Dyson, *Inorg. Chem. Commun.*, **10**, 558 (2007).
127. M. Nunes da Ponte and M. E. Zakrzewska, *The Journal of Supercritical Fluids*, **113**, 61 (2016).
128. S. P. Verevkin, D. H. Zaitsau, V. N. Emelỳanenko, and A. Heintz, *J. Phys. Chem. B*, **115**, 12889 (2011).
129. M. Klähn and A. Seduraman, *J. Phys. Chem. B*, **119**, 10066 (2015).
130. V. K. Shen, D. W. Siderius, W. P. Krekelberg, and H. W. Hatch, (2017), NIST Standard Reference Simulation Website, NIST Standard Reference Database Number 173, National Institute of Standards and Technology, Gaithersburg MD, 20899 (retrieved June 23, 2021), http://doi.org/10.18434/T4M88Q.
131. S. N. V. K. Aki, B. R. Mellein, E. M. Saurer, and J. F. Brennecke, *J. Phys. Chem. B*, **108**, 20355 (2004).
132. W. Ren, B. Sensenich, and A. M. Scurto, *The Journal of Chemical Thermodynamics*, **42**, 305 (2010).
133. I. Mejía, K. Stanley, R. Canales, and J. F. Brennecke, *Journal of Chemical & Engineering Data*, **58**, 2642 (2013).
134. J. Palgunadi, J. E. Kang, D. Q. Nguyen, J. H. Kim, B. K. Min, S. D. Lee, H. Kim, and H. S. Kim, *Thermochim. Acta*, **494**, 94 (2009).
135. Y. S. Kim, J. H. Jang, B. D. Lim, J. W. Kang, and C. S. Lee, *Fluid Phase Equilib.*, **256**, 70 (2007).
136. L. Zhou, J. Fan, X. Shang, and J. Wang, *The Journal of Chemical Thermodynamics*, **59**, 28 (2013).
137. M. B. Shiflett and A. Yokozeki, *Ind. Eng. Chem. Res.*, **44**, 4453 (2005).
138. T. Nonthanasin, A. Henni, and C. Saiwan, *RSC Adv.*, **4**, 7566 (2014).
139. S. Raeissi, L. Florusse, and C. J. Peters, *The Journal of Supercritical Fluids*, **55**, 825 (2010).
140. R. L. Scott and P. H. van Konynenburg, *Discuss. Faraday Soc.*, **49**, 87 (1970).
141. M. B. Shiflett, A. M. S. Niehaus, and A. Yokozeki, *Journal of Chemical & Engineering Data*, **55**, 4785 (2010).
142. M. B. Shiflett and A. Yokozeki, *Journal of Chemical & Engineering Data*, **54**, 108 (2009).
143. S. G. Kazarian, B. J. Briscoe, and T. Welton, *Chem. Commun.*, 2047 (2020).
144. A. L. Chaffee, G. P. Knowles, Z. Liang, J. Zhang, P. Xiao, and P. A. Webley, *Int. J. Greenhouse Gas Control*, **5**, 1368 (2011).
145. L. Delaude and A. Synth, *Catal.*, **362**, 3259 (2020).
146. B. Arstad, R. Blom, and O. Swang, *The Journal of Physical Chemistry A*, **111**, 1222 (2007).
147. J. E. Crooks and J. P. Donnellan, *Journal of the Chemical Society, Perkin Transactions*, **2**, 331 (1989).
148. P. J. Carvalho, K. A. Kurnia, and J. A. P. Coutinho, *Phys. Chem. Chem. Phys.*, **18**, 14757 (2016).
149. F. Vega, F. M. Baena-Moreno, L. M. Gallego Fernández, E. Portillo, B. Navarrete, and Z. Zhang, *Appl. Ener.*, **260**, 114313 (2020).

150. M. B. Shiflett, D. J. Kasprzak, C. P. Junk, and A. Yokozeki, *The Journal of Chemical Thermodynamics*, **40**, 25 (2008).
151. P. J. Carvalho, V. H. Álvarez, B. Schröder, A. M. Gil, I. M. Marrucho, M. Aznar, L. M. N. B. F. Santos, and J. A. P. Coutinho, *J. Phys. Chem. B*, **113**, 6803 (2009).
152. Y. Huang, G. Cui, H. Wang, Z. Li, and J. Wang, *Journal of CO2 Utilization*, **28**, 299 (2018).
153. M. B. Shiflett, D. W. Drew, R. A. Cantini, and A. Yokozeki, *Energy & Fuels*, **24**, 5781 (2010).
154. N. M. Simon, M. Zanatta, F. P. dos Santos, M. C. Corvo, E. J. Cabrita, and J. Dupont, *, Chem. Sus. Chem*, **10**, 4927 (2017).
155. E. Pérez, L. de Pablo, J. J. Segovia, A. Moreau, F. A. Sánchez, S. Pereda, and M. D. Bermejo, *AIChE J.*, **66**, e16228 (2020).
156. C. Ma, S. Sarmad, J.-P. Mikkola, and X. Ji, *Energy Procedia*, **142**, 3320 (2017).
157. A. Yokozeki, M. B. Shiflett, C. P. Junk, L. M. Grieco, and T. Foo, *J. Phys. Chem. B*, **112**, 16654 (2008).
158. E. Torralba-Calleja, J. Skinner, and D. Gutiérrez-Tauste, *Journal of Chemistry*, **2013**, 473584 (2013).
159. M. Ramdin, A. Amplianitis, S. Bazhenov, A. Volkov, V. Volkov, T. J. H. Vlugt, and T. W. de Loos, *Ind. Eng. Chem. Res.*, **53**, 15427 (2014).
160. E. Kühne, E. Perez, G. J. Witkamp, and C. J. Peters, *The Journal of Supercritical Fluids*, **45**, 27 (2008).
161. S. Jang, D.-W. Cho, T. Im, and H. Kim, *Fluid Phase Equilib.*, **299**, 216 (2010).
162. P. J. Carvalho, V. H. Álvarez, I. M. Marrucho, M. Aznar, and J. A. P. Coutinho, *The Journal of Supercritical Fluids*, **50**, 105 (2009).
163. R. B. Leron, A. N. Soriano, and M.-H. Li, *J. Taiwan Inst. Chem. Eng.*, **43**, 551 (2012).
164. H. Liu, J. Huang, and P. Pendleton, *Energy Procedia*, **4**, 59 (2011).
165. F. Dreisbach and H. W. Lösch, *J. Therm. Anal. Calorim.*, **62**, 515 (2000).
166. M. Petermann, T. Weissert, S. Kareth, H. W. Lösch, and F. Dreisbach, *The Journal of Supercritical Fluids*, **45**, 156 (2008).
167. A. N. Soriano, B. T. Doma, and M.-H. Li, *Journal of Chemical & Engineering Data*, **53**, 2550 (2008).
168. P. G. Jessop and B. Subramaniam, *Chem. Rev.*, **107**, 2666 (2007).
169. B. Yu, H. Yu, Q. Yang, K. Li, L. Ji, R. Zhang, M. Megharaj, and Z. Chen, *Energy & Fuels*, **33**, 7500 (2019).
170. P. D. Vaidya and E. Y. Kenig, *Chem. Eng. Sci.*, **62**, 7344 (2007).
171. K. Li, H. Yu, M. Tade, P. Feron, J. Yu, and S. Wang, *Environmental Science & Technology*, **48**, 7179 (2014).
172. K. Li, H. Yu, S. Yan, P. Feron, L. Wardhaugh, and M. Tade, *Environmental Science & Technology*, **50**, 10746 (2016).
173. S. Sarmad, J.-P. Mikkola, and X. Ji, *ChemSusChem*, **10**, 324 (2017).
174. C. D'Agostino, R. C. Harris, A. P. Abbott, L. F. Gladden, and M. D. Mantle, *Phys. Chem. Chem. Phys.*, **13**, 21383 (2011).
175. L. F. Zubeir, C. Held, G. Sadowski, and M. C. Kroon, *J. Phys. Chem. B*, **120**, 2300 (2016).
176. H. Bai and A. C. Yeh, *Ind. Eng. Chem. Res.*, **36**, 2490 (1997).
177. X. Liu, Y. Chen, S. Zeng, X. Zhang, S. Zhang, X. Liang, R. Gani, and G. M. Kontogeorgis, *AIChE J.*, **66**, e16794 (2020).
178. X. Liu, Y. Huang, Y. Zhao, R. Gani, X. Zhang, and S. Zhang, *Ind. Eng. Chem. Res.*, **55**, 5931 (2016).
179. P. Navarro, J. García, F. Rodríguez, P. J. Carvalho, and J. A. P. Coutinho, *Journal of CO2 Utilization*, **31**, 115 (2019).
180. M. E. Zakrzewska and M. Nunes da Ponte, *Journal of Chemical & Engineering Data*, **63**, 907 (2018).
181. L. M. C. Oliveira, F. R. G. Ribeiro, M. L. Alcantara, G. O. Pisoni, V. F. Cabral, L. Cardozo-Filho, and S. Mattedi, *Fluid Phase Equilib.*, **426**, 65 (2016).
182. P. J. Carvalho, V. H. Álvarez, I. M. Marrucho, M. Aznar, and J. A. P. Coutinho, *The Journal of Supercritical Fluids*, **52**, 258 (2010).
183. M. L. Alcantara, M. L. de Carvalho, V. H. Álvarez, P. I. S. Ferreira, M. L. L. Paredes, L. Cardozo-Filho, A. K. Silva, L. M. Lião, C. A. M. Pires, and S. Mattedi, *Fluid Phase Equilib.*, **460**, 162 (2018).
184. J. O. Valderrama and R. E. Rojas, *Ind. Eng. Chem. Res.*, **48**, 6890 (2009).
185. J. O. Valderrama and R. E. Rojas, *Fluid Phase Equilib.*, **297**, 107 (2010).
186. G. M. Bollas, C. C. Chen, and P. I. Barton, *AIChE J.*, **54**, 1608 (2008).
187. A. Mohs and J. Gmehling, *Fluid Phase Equilib.*, **337**, 311 (2013).
188. M. Jaschik, D. Piech, K. Warmuzinski, and J. Jaschik, *Chemical and Process Engineering*, **38**, 19 (2017).
189. D. Camper, J. Bara, C. Koval, and R. Noble, *Ind. Eng. Chem. Res.*, **45**, 6279 (2006).
190. D. Camper, P. Scovazzo, C. Koval, and R. Noble, *Ind. Eng. Chem. Res.*, **43**, 3049 (2004).
191. P. Scovazzo, D. Camper, J. Kieft, J. Poshusta, C. Koval, and R. Noble, *Ind. Eng. Chem. Res.*, **43**, 6855 (2004).
192. D. Camper, C. Becker, C. Koval, and R. Noble, *Ind. Eng. Chem. Res.*, **44**, 1928 (2005).
193. A. Erriguible, S. Vincent, and P. Subra-Paternault, *The Journal of Supercritical Fluids*, **63**, 16 (2012).
194. X. Yuan, S. Zhang, J. Liu, and X. Lu, *Fluid Phase Equilib.*, **257**, 195 (2007).
195. A. G. Georgiadis, N. D. Charisiou, and M. A. Goula, *Catalysts*, **10** (2020).
196. M. Hosseini, R. Rahimi, and M. Ghaedi, *J. Mol. Liq.*, **317**, 113984 (2020).
197. J. M. M. V. Sousa, T. E. Sintra, A. G. M. Ferreira, P. J. Carvalho, and I. M. A. Fonseca, *The Journal of Chemical Thermodynamics*, **154**, 106336 (2021).
198. A. H. Jalili, M. Safavi, C. Ghotbi, A. Mehdizadeh, M. Hosseini-Jenab, and V. Taghikhani, "The." *J. Phys. Chem. B*, **116**, 2758 (2012).
199. X. Wang, S. Zeng, J. Wang, D. Shang, X. Zhang, J. Liu, and Y. Zhang, *Ind. Eng. Chem. Res.*, **57**, 1284 (2018).
200. H. Handy, A. Santoso, A. Widodo, J. Palgunadi, T. H. Soerawidjaja, and A. Indarto, *Sep. Sci. Technol.*, **49**, 2079 (2014).
201. J. Wang, Z. Song, H. Cheng, L. Chen, L. Deng, and Z. Qi, *Sep. Purif. Technol.*, **248**, 117053 (2020).
202. M. Taheri, R. Zhu, G. Yu, and Z. Lei, *Chem. Eng. Sci.*, **230**, 116199 (2021).
203. F.-Y. Jou and A. E. Mather, *Int. J. Thermophys.*, **28**, 490 (2007).
204. A. Amhamed, M. Atilhan, and G. Berdiyorov, *Molecules* (Basel, Switzerland) 24 (2019).
205. T. Zhao, P. Li, X. Feng, X. Hu, and Y. Wu, *J. Mol. Liq.*, **266**, 806 (2018).
206. H. Wu, M. Shen, X. Chen, G. Yu, A. A. Abdeltawab, and S. M. Yakout, *Sep. Purif. Technol.*, **224**, 281 (2019).
207. X. Zhang, W. Xiong, L. Peng, Y. Wu, and X. Hu, *AIChE J.*, **66**, e16936 (2020).
208. J. Tian and B. Liu, *Critical Reviews in Environmental Science and Technology*, **1** (2020).
209. T. Makino and M. Kanakubo, *New J. Chem.*, **44**, 20665 (2020).
210. M. Yu, S. Zeng, Z. Wang, Z. Hu, H. Dong, Y. Nie, B. Ren, and X. Zhang, *ACS Sustainable Chem. & Eng.*, **7**, 11769 (2019).
211. K. N. Ruckart, Y. Zhang, W. M. Reichert, G. W. Peterson, and T. G. Glover, *Ind. Eng. Chem. Res.*, **55**, 12191 (2016).
212. J. Lemus, J. Bedia, C. Moya, N. Alonso-Morales, M. A. Gilarranz, J. Palomar, and J. J. Rodriguez, *RSC Adv.*, **6**, 61650 (2016).
213. R. Qiu, X. Luo, L. Yang, J. Li, X. Chen, C. Peng, and J. Lin, *ACS Sustainable Chem. & Eng.*, **8**, 1637 (2020).
214. F. T. U. Kohler, S. Popp, H. Klefer, I. Eckle, C. Schrage, B. Böhringer, D. Roth, M. Haumann, and P. Wasserscheid, *Green Chem.*, **16**, 3560 (2014).
215. D. Fu, X. Sun, J. Pu, and S. Zhao, *Journal of Chemical & Engineering Data*, **51**, 371 (2006).
216. M. D. Bermejo, M. Montero, E. Saez, L. J. Florusse, A. J. Kotlewska, M. J. Cocero, F. van Rantwijk, and C. J. Peters, *J. Phys. Chem. B*, **112**, 13532 (2008).
217. Z. Dai, R. D. Noble, D. L. Gin, X. Zhang, and L. Deng, *J. Membr. Sci.*, **497**, 1 (2016).
218. G. M. Avelar Bonilla, O. Morales-Collazo, and J. F. Brennecke, *ACS Sustainable Chem. & Eng.*, **7**, 16858 (2019).
219. M. Zanatta, N. M. Simon, F. P. dos Santos, M. C. Corvo, E. J. Cabrita, and J. Dupont, *Angew. Chem. Int. Ed.*, **58**, 382 (2019).
220. N. S. Sifat and Y. Haseli, *Energies*, **12** (2019).
221. J. Leclaire and D. J. Heldebrant, *Green Chem.*, **20**, 5058 (2018).
222. A. L. Kohl and R. Nielson, *Gas Purification* (Gulf Professional Publishing, Houston, Texas, United States of America) (1997).
223. P. J. M. Carvalho, "Tratamento De Correntes De Gás Natural Com Líquidos Iónicos." *Departamento de química* (Universidade de Aveiro, Aveio, Portugal) (2011).
224. H. Wu, X. Li, Y. Li, S. Wang, R. Guo, Z. Jiang, C. Wu, Q. Xin, and X. Lu, *J. Membr. Sci.*, **465**, 78 (2014).
225. R. Ur Rehman, S. Rafiq, N. Muhammad, A. L. Khan, A. Ur Rehman, L. TingTing, M. Saeed, F. Jamil, M. Ghauri, and X. Gu, *J. Appl. Polym. Sci.*, **134**, 45395 (2017).
226. A. A. Taimoor, S. Al-Shahrani, and A. Muhammad, *Processes*, **6** (2018).
227. S. D. Sharma and M. Azzi, *Fuel*, **121**, 178 (2014).
228. G. Hu, N. J. Nicholas, K. H. Smith, K. A. Mumford, S. E. Kentish, and G. W. Stevens, *Int. J. Greenhouse Gas Control*, **53**, 28 (2016).
229. D. S. Firaha and B. Kirchner, *Chem. Sus. Chem*, **9**, 1591 (2016).
230. A. F. Portugal, J. M. Sousa, F. D. Magalhães, and A. Mendes, *Chem. Eng. Sci.*, **64**, 1993 (2009).
231. A. L. Yaumi, M. Z. A. Bakar, and B. H. Hameed, *Energy*, **124**, 461 (2017).
232. Y.-C. Chiang and R.-S. Juang, *J. Taiwan Inst. Chem. Eng.*, **71**, 214 (2017).
233. V. Irani, A. Maleki, and A. Tavasoli, *J. Environ. Chem. Eng.*, **7**, 102782 (2019).
234. N. Hsan, P. K. Dutta, S. Kumar, R. Bera, and N. Das, *Int. J. Biol. Macromol.*, **125**, 300 (2019).
235. J. Li, X. Zhou, L. Zhang, H. Di, H. Wu, and L. Yang, *Energy & Fuels*, **31**, 778 (2017).
236. C. Florindo, L. Romero, I. Rintoul, L. C. Branco, and I. M. Marrucho, *ACS Sustainable Chem. & Eng.*, **6**, 3888 (2018).
237. S. Seo, L. D. Simoni, M. Ma, M. A. DeSilva, Y. Huang, M. A. Stadtherr, and J. F. Brennecke, *Energy & Fuels*, **28**, 5968 (2014).
238. S. Zhang, Y. Shen, L. Wang, J. Chen, and Y. Lu, *Appl. Ener.*, **239**, 876 (2019).
239. P. G. Jessop, D. J. Heldebrant, X. Li, C. A. Eckert, and C. L. Liotta, *Nature*, **436**, 1102 (2005).
240. P. G. Jessop, S. M. Mercer, and D. J. Heldebrant, *Energy Environ. Sci.*, **5**, 7240 (2012).
241. X. Li, Q. Xu, H. Shen, Y. Guo, M. Wu, Y. Peng, L. Zhang, Z. K. Zhao, Y. Liu, and H. Xie, *Carbohydr. Polym.*, **204**, 50 (2019).
242. X. Zhu, M. Song, and Y. Xu, *ACS Sustainable Chem. & Eng.*, **5**, 8192 (2017).
243. Y. Huang, G. Cui, Y. Zhao, H. Wang, Z. Li, S. Dai, and J. Wang, *Angew. Chem. Int. Ed.*, **56**, 13293 (2017).
244. D. Hospital-Benito, J. Lemus, C. Moya, R. Santiago, and J. Palomar, *Chem. Eng. J.*, **390**, 124509 (2020).
245. V. Abetz et al., *Adv. Eng. Mater.*, **8**, 328 (2006).
246. H. B. Park, J. Kamcev, L. M. Robeson, M. Elimelech, and B. D. Freeman, *Science*, **356**, eaab0530 (2017).
247. S. Wang et al., *Energy Environ. Sci.*, **9**, 1863 (2016).
248. D. L. Gin and R. D. Noble, *Science*, **332**, 674 (2011).
249. H. Lin and B. D. Freeman, *J. Mol. Struct.*, **739**, 57 (2005).
250. Z. Lai et al., *Science*, **300**, 456 (2003).
251. R. T. Adams, J. S. Lee, T.-H. Bae, J. K. Ward, J. R. Johnson, C. W. Jones, S. Nair, and W. J. Koros, *J. Membr. Sci.*, **367**, 197 (2011).
252. B. Mi, *Science*, **343**, 740 (2014).

253. H. B. Park and Y. M. Lee, *Adv. Mater.*, **17**, 477 (2005).
254. M. Z. Ahmad, T. A. Peters, N. M. Konnertz, T. Visser, C. Téllez, J. Coronas, V. Fila, W. M. de Vos, and N. E. Benes, *Sep. Purif. Technol.*, **230**, 115858 (2020).
255. J. Peter, M. A. Khalyavina, J. Kříž, and M. Bleha, *Eur. Polym. J.*, **45**, 1716 (2009).
256. L. Wang, Y. Cao, M. Zhou, S. J. Zhou, and Q. Yuan, *J. Membr. Sci.*, **305**, 338 (2007).
257. J. R. Wiegand, Z. P. Smith, Q. Liu, C. T. Patterson, B. D. Freeman, and R. Guo, *J. Mater. Chem. A*, **2**, 13309 (2014).
258. C. Camacho-Zuñiga, F. A. Ruiz-Treviño, S. Hernández-López, M. G. Zolotukhin, F. H. J. Maurer, and A. González-Montiel, *J. Membr. Sci.*, **340**, 221 (2009).
259. A. Jomekian, S. A. A. Mansoori, N. Monirimanesh, and A. Shafiee, *Korean J. Chem. Eng.*, **28**, 2069 (2011).
260. S. Li, H. J. Jo, S. H. Han, C. H. Park, S. Kim, P. M. Budd, and Y. M. Lee, *J. Membr. Sci.*, **434**, 137 (2013).
261. T.-H. Weng, H.-H. Tseng, and M.-Y. Wey, *J. Membr. Sci.*, **369**, 550 (2011).
262. R. Castro-Muñoz and V. Fíla, "Progress on Incorporating Zeolites in Matrimid®5218 Mixed matrix membranes towards gas separation." *Membranes* (2018).
263. A. Nogalska, A. Trojanowska, and R. Garcia-Valls, *Physical Sciences Reviews*, **2**, 20170059 (2017).
264. X. Yan, S. Anguille, M. Bendahan, and P. Moulin, *Sep. Purif. Technol.*, **222**, 230 (2019).
265. A. Alkhouzaam, M. Khraisheh, M. Atilhan, S. A. Al-Muhtaseb, L. Qi, and D. Rooney, *J. Nat. Gas Sci. Eng.*, **36**, 472 (2016).
266. M. L. Alcantara, G. de Almeida Oliveira, L. M. Lião, C. P. Borges, and S. Mattedi, *Ind. Eng. Chem. Res.*, **60**, 4405 (2021).
267. H. Bai and W. S. W. Ho, *Ind. Eng. Chem. Res.*, **48**, 2344 (2009).
268. M. Mohammadi, M. Asadollahzadeh, and S. Shirazian, *J. Mol. Liq.*, **262**, 230 (2018).
269. Y. Liu, S. Yu, H. Wu, Y. Li, S. Wang, Z. Tian, and Z. Jiang, *J. Membr. Sci.*, **469**, 198 (2014).
270. C. Myers, H. Pennline, D. Luebke, J. Ilconich, J. K. Dixon, E. J. Maginn, and J. F. Brennecke, *J. Membr. Sci.*, **322**, 28 (2008).
271. H. B. Park, C. H. Jung, Y. M. Lee, A. J. Hill, S. J. Pas, S. T. Mudie, E. Van Wagner, B. D. Freeman, and D. J. Cookson, *Science*, **318**, 254 (2007).
272. T. K. Carlisle, J. E. Bara, A. L. Lafrate, D. L. Gin, and R. D. Noble, *J. Membr. Sci.*, **359**, 37 (2010).
273. Z. Dai, L. Ansaloni, and L. Deng, *Green Ener. & Environ.*, **1**, 102 (2016).
274. J. E. Bara, C. J. Gabriel, E. S. Hatakeyama, T. K. Carlisle, S. Lessmann, R. D. Noble, and D. L. Gin, *J. Membr. Sci.*, **321**, 3 (2008).
275. C. A. Dunn, S. Denning, J. M. Crawford, R. Zhou, G. E. Dwulet, M. A. Carreon, D. L. Gin, and R. D. Noble, *J. Membr. Sci.*, **621**, 118979 (2021).
276. M. G. Cowan, D. L. Gin, and R. D. Noble, *Acc. Chem. Res.*, **49**, 724 (2016).
277. B. Lam, M. Wei, L. Zhu, S. Luo, R. Guo, A. Morisato, P. Alexandridis, and H. Lin, *Polym.*, **89**, 1 (2016).
278. C. S. K. Achoundong, N. Bhuwania, S. K. Burgess, O. Karvan, J. R. Johnson, and W. J. Koros, *Macromolecules*, **46**, 5584 (2013).
279. L. Deng, T.-J. Kim, and M.-B. Hägg, *J. Membr. Sci.*, **340**, 154 (2009).
280. Z. Liu, C. Liu, L. Li, W. Qin, and A. Xu, *Int. J. Greenhouse Gas Control*, **53**, 79 (2016).
281. T. Oncsik, R. Vijayaraghavan, and D. R. MacFarlane, *Chem. Commun.*, **54**, 2106 (2018).
282. C.-H. Lim, A. M. Holder, J. T. Hynes, and C. B. Musgrave, *JACS*, **136**, 16081 (2014).
283. C.-H. Lim, S. Ilic, A. Alherz, B. T. Worrell, S. S. Bacon, J. T. Hynes, K. D. Glusac, and C. B. Musgrave, *JACS*, **141**, 272 (2019).
284. Z. A. S. Bairq, H. Gao, F. A. M. Murshed, P. Tontiwachwuthikul, and Z. Liang, *ACS Sustainable Chem. & Eng.*, **8**, 9526 (2020).
285. M. S. Alivand, O. Mazaheri, Y. Wu, G. W. Stevens, C. A. Scholes, and K. A. Mumford, *ACS Sustainable Chem. & Eng.*, **8**, 18755 (2020).
286. A. Weilhard, M. I. Qadir, V. Sans, and J. Dupont, *ACS Catal.*, **8**, 1628 (2018).
287. D. V. Vasilyev and P. J. Dyson, *ACS Catal.*, **1392** (2021).
288. M. H. Mamme, S. L. C. Moors, E. A. Mernissi Cherigui, H. Terryn, J. Deconinck, J. Ustarroz, and F. De, *Proft, Nanoscale Advances*, **1**, 2847 (2019).
289. Y. Meng, L. Aldous, S. R. Belding, and R. G. Compton, *Chem. Commun.*, **48**, 5572 (2012).
290. L. E. Barrosse-Antle, A. M. Bond, R. G. Compton, A. M. O'Mahony, E. I. Rogers, and D. S. Silvester, *Chem.—Asian J.*, **5**, 202 (2010).
291. Y. Meng, S. Norman, C. Hardacre, and R. G. Compton, *Phys. Chem. Chem. Phys.*, **15**, 2031 (2013).
292. C. Fu, L. Aldous, E. J. F. Dickinson, N. S. A. Manan, and R. G. Compton, *New J. Chem.*, **36**, 774 (2012).
293. E. I. Rogers, B. Šljukić, C. Hardacre, and R. G. Compton, *Journal of Chemical & Engineering Data*, **54**, 2049 (2009).
294. E. I. Rogers, D. S. Silvester, D. L. Poole, L. Aldous, C. Hardacre, and R. G. Compton, *J. Phys. Chem. C*, **112**, 2729 (2008).
295. E. I. Rogers, D. S. Silvester, S. E. Ward Jones, L. Aldous, C. Hardacre, A. J. Russell, S. G. Davies, and R. G. Compton, *J. Phys. Chem. C*, **111**, 13957 (2007).
296. M. C. Buzzeo, C. Hardacre, and R. G. Compton, *Chem. Phys. Chem.*, **7**, 176 (2006).
297. C. A. Paddon and R. G. Compton, *Electroanalysis*, **17**, 1919 (2005).
298. G. Gritzner and J. Kuta, *Pure Appl. Chem.*, **54**, 1527 (1982).
299. G. Gritzner and J. Kuta, *Pure Appl. Chem.*, **56**, 461 (1984).
300. M. J. A. Shiddiky, A. A. J. Torriero, C. Zhao, I. Burgar, G. Kennedy, and A. M. Bond, *JACS*, **131**, 7976 (2009).
301. S. K. Sukardi, J. Zhang, I. Burgar, M. D. Horne, A. F. Hollenkamp, D. R. MacFarlane, and A. M. Bond, *Electrochem. Commun.*, **10**, 250 (2008).
302. C. Fu, L. Aldous, E. J. F. Dickinson, N. S. A. Manan, and R. G. Compton, *Chem. Commun.*, **47**, 7083 (2011).
303. L. E. Barrosse-Antle, L. Aldous, C. Hardacre, A. M. Bond, and R. G. Compton, *J. Phys. Chem. C*, **113**, 7750 (2009).
304. U. Schröder, J. D. Wadhawan, R. G. Compton, F. Marken, P. A. Z. Suarez, C. S. Consorti, R. F. de Souza, and J. Dupont, *New J. Chem.*, **24**, 1009 (2000).
305. Y. Meng, L. Aldous, S. R. Belding, and R. G. Compton, *Phys. Chem. Chem. Phys.*, **14**, 5222 (2012).
306. N. G. Connelly and W. E. Geiger, *Chem. Rev.*, **96**, 877 (1996).
307. B. Tang, R. Gondosiswanto, D. B. Hibbert, and C. Zhao, *Electrochim. Acta*, **298**, 413 (2019).
308. X. Lu, G. Burrell, F. Separovic, and C. Zhao, *J. Phys. Chem. B*, **116**, 9160 (2012).
309. Y. Chen and T. Mu, *Green Chem.*, **21**, 2544 (2019).
310. D. Faggion Jr, W. D. G. Gonçalves, and J. Dupont, *Frontiers in Chemistry*, **7**, 102 (2019).
311. W. D. G. Gonçalves, M. Zanatta, N. M. Simon, L. M. Rutzen, D. A. Walsh, and J. Dupont, *Chem. Sus. Chem.*, **12**, 4170 (2019).
312. J. T. Feaster, A. L. Jongerius, X. Liu, M. Urushihara, S. A. Nitopi, C. Hahn, K. Chan, J. K. Nørskov, and T. F. Jaramillo, *Langmuir: the ACS journal of surfaces and colloids*, **33**, 9464 (2017).
313. L. Sun, G. K. Ramesha, P. V. Kamat, and J. F. Brennecke, *Langmuir: the ACS journal of surfaces and colloids*, **30**, 6302 (2014).
314. Y. Hori, *Modern Aspects of Electrochemistry*, ed. C. G. Vayenas, R. E. White, and M. E. Gamboa-Aldeco et al. (Springer, New York, NY) p. 89 (2008), https://www.springer.com/gp/book/9780387494883.
315. A. Y. Khodakov, W. Chu, and P. Fongarland, *Chem. Rev.*, **107**, 1692 (2007).
316. C. J. Weststrate, J. van de Loosdrecht, and J. W. Niemantsverdriet, *J. Catal.*, **342**, 1 (2016).
317. C. J. Weststrate, P. van Helden, and J. W. Niemantsverdriet, *Catal. Today*, **275**, 100 (2016).
318. D. Gao, I. Zegkinoglou, N. J. Divins, F. Scholten, I. Sinev, P. Grosse, and B Roldan Cuenya, *ACS Nano*, **11**, 4825 (2017).
319. L. Cao, P. Zhu, Y. Zhao, and J. Zhao, *J. Hazard. Mater.*, **352**, 17 (2018).
320. S. Lee, D. Kim, and J. Lee, *Angew. Chem.*, **127**, 14914 (2015).
321. K. P. Kuhl, E. R. Cave, D. N. Abram, and T. F. Jaramillo, *Energy Environ. Sci.*, **5**, 7050 (2012).
322. K. Lv, Y. Fan, Y. Zhu, Y. Yuan, J. Wang, Y. Zhu, and Q. Zhang, *J. Mater. Chem. A*, **6**, 5025 (2018).
323. L. Ji, L. Chang, Y. Zhang, S. Mou, T. Wang, Y. Luo, Z. Wang, and X. Sun, *ACS Catal.*, **9**, 9721 (2019).
324. H. Mistry et al., *Nat. Commun.*, **77**, 12123 (2016).
325. X. Wang et al., *Nat. Commun.*, **10**, 5186 (2019).
326. K. Ito, S. Ikeda, T. Iida, and A. Nomura, *Denki Kagaku*, **50**, 463 (1982).
327. A. Mota-Lima, *J. Phys. Chem. C*, **124**, 10907 (2020).
328. M. Ramdin, A. R. T. Morrison, M. de Groen, R. van Haperen, R. de Kler, L. J. P. van den Broeke, J. P. M. Trusler, W. de Jong, and T. J. H. Vlugt, *Ind. Eng. Chem. Res.*, **58**, 1834 (2019).